Geothermics 106 (2022) 102552

Contents lists available at ScienceDirect

Geothermics

journal homepage: www.elsevier.com/locate/geothermics

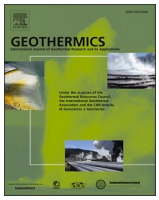

Hot water-methane reservoirs at southwest foothills of Koryaksky volcano, Kamchatka

A.V. Kiryukhin [a,*], I.N. Nazhalova [b], N.B. Zhuravlev [a]

[a] Institute of Volcanology and Seismology FEB RAS, Petropavlovsk-Kamchatsky, Piip-9, 683006 Russia
[b] Zarechnoe JSC, Kamchatsky Krai, Elizovsky District, Razdolny, Tayozhnaya 2, 684020 Russia

ARTICLE INFO

Keywords:
Volcano, hydrothermal
Modeling
Geofluids
CH_4
Fracking
Ketkinsky
Gas
Reservoir
iTOUGH2
TOUGH2-EWASG
Kamchatka

ABSTRACT

A conceptual model of the thermal and water recharge of the Ketkinsky geothermal field as a product of magma and water injection from the Koryaksky volcano located 24 km apart was proposed. A digital hydrogeological model of the Ketkinsky geothermal field was developed in the volume of 7 km x 5 km x 2.5 km (from the topographic surface), it includes the space drilled by exploration and production wells. The model is based on an analysis of 3D distributions of temperature, pressure, salinity and CH_4 content, geometrization of productive faults and well productivity characteristics. The geofiltration space was zoned in the model with separation of deep and shallow productive geothermal reservoirs, the area of deep thermal fluid upflow in the SSE part of the model base and the area of hidden thermal water discharge at the ground surface.

A natural state inversion iTOUGH2-EWASG simulation was performed to estimate the deep thermal water upflow and permeability of productive geothermal reservoirs. The deep thermal water upflow is estimated to be about 10 kg/s, the permeability is estimated to be 190 mD (shallow productive reservoir) and 35 mD (deep productive reservoir). Inverse iTOUGH2-EWASG modeling of the hydrodynamic operating history of 1989–2020 was used to estimate the compressibility of the productive geothermal reservoirs: the compressibility of the deep reservoir is estimated at 7.16E-10 Pa^{-1}, the shallow reservoir at 4.14E-07 Pa^{-1}. Direct iTOUGH2-EWASG modeling with the above parameters reproduces the history of salinity and temperature changes in production wells.

Forecast modeling of existing producing wells #23, K6, K01, K5 operation for 25 years with application of submersible pumps at immersion depth of 70 m confirms the possibility of their sustainable operation with total flow rate not less than 14.2 kg/s, adding four producing wells may yield to 54.3 kg/s with retaining of produced water quality (temperature, gas content of CH_4, salinity).

The use of submersible pumps and reinjection can significantly increase the reserves of Ketkinsky field to 165–175 kg/s of 70–80 °C and 60–70 g/s of CH_4. Additional increase in reserves may be obtained by drilling the already known thermal anomaly in the SSE sector of the field and in the SWW foothills of Koryaksky volcano.

1. Introduction

Ketkinsky geothermal field was formed on the western margin of the Avachinsky-Koryaksky volcanogenic basin with an area of 2530 km^2. The mentioned basin includes 5 quaternary volcanoes (two of which Avachinsky (2750 m) and Koryaksky (3456 m) are active), sub-basins of volcanogenic-sedimentary Neogene-Quaternary sediments up to 1.4 km thick (Figs. 1 and 2). The basin is located in a depression formed in the upper part of the basement of pre-Cretaceous age, characterized by a low temperature gradient of 24 °C/km. The basin foundation is composed of Upper Cretaceous K_2 and Upper Jurassic J_3 sediments, which are represented by metamorphic rocks with low porosity and permeability in general, but local fractured zones are present, from which well tests have yielded water rates of up to 6 kg/s in the depth interval 1438–1490 m (well E1) (Posdeev, 2003). The average thermal conductivity of Cretaceous-age rocks is 2.8 W/m/°C. The Neogene-Lower Quaternary aquifer complex is composed of pyroclastic and volcanogenic-sedimentary formations. The porosity values are rather high: 0.36÷0.48, specific well flow rates are up to 0.01 l/s/m (wells GK-1, Pinachevsky). The aquiferous complex of the Pinachevo extrusive

* Corresponding author.
E-mail address: AVKiryukhin2@mail.ru (A.V. Kiryukhin).

https://doi.org/10.1016/j.geothermics.2022.102552
Received 9 May 2022; Received in revised form 16 August 2022; Accepted 22 August 2022
Available online 22 September 2022

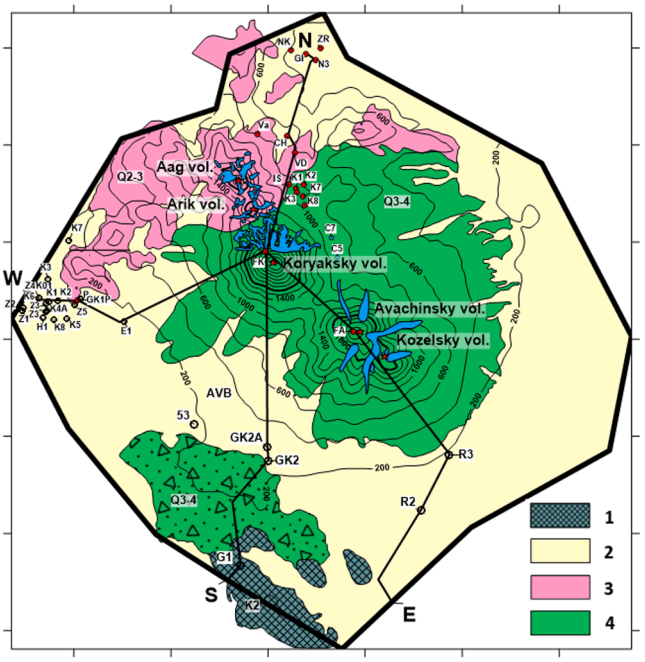

Fig. 1. Schematic geological map of the Koryaksky-Avachinsky volcanogenic basin.
Legend (geological units): 1 - basement rocks of Cretaceous age and older (K_2), 2 - volcanogenic-sedimentary Neogene-Quaternary (N-Q_1) deposits, 3 - sub-basin of Pinachevsky extrusions (Q_{2-3}), 4 - Avachnsky, Koryaksky, Kozelsky volcanoes and volcanic eruptions products near Petropavlovsk-Kamchatsky (Q_{3-4}).
Hydrogeological features: Thermal mineral springs (shown by filled circles): K1, K2, K3, K7, K8 - Koryaksky Narzan, IS - Izotovsky, VD - Vodopadny, CH - Chistinsky, Va - Vakinsky, N3 - Nalychevsky (Luzha-3), GI - Ivanov Griffon, NK - Nalychevsky Boiler, ZR - Zheltorechensky, P - Pinachevsky. Fumaroles: FK-Koryaksky, FA - Avachinsky. Cold springs: C5 and C7. AVB - artesian-volcanic basin. Wells are shown uncolored circles with corresponding numbers.
WE and SN are geological section lines. The axis markings are 10 km.

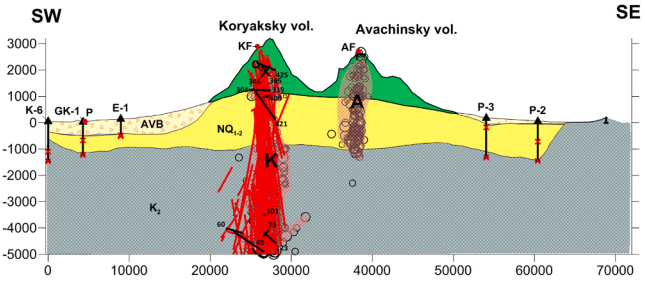

Fig. 2. Geological cross-section of the Koryaksky-Avachinsky volcanogenic basin along the southwestern-southeastern line (SW-SE, position of the section is shown in Fig. 1). The section shows circles, which are hypocenters of local earthquakes in the period from 2008 to 2019 (data from KB FRC UGS RAS). Additionally, red lines show injections of dikes and sills during time period above mentioned in the vertical section of well Z1 - FK (see Fig. 1). Low angle dikes/sills with dip angles below 30° are shown in black and numbered. Sills 60 and 49 may be involved in the formation of thermally-fluid feeding faults for the Ketkinsky geothermal field, given that the water recharge area of the Koryaksky-Avachinsky volcanogenic basin includes structures of volcanoes (see Section 2.2).

massif Q_{2-3} is composed of andesite and rhyolite extrusions and includes vent formations of andesites, dacites and rhyolites (thickness more than 200–500 m). According to laboratory studies, the porosity is 0.12, permeability 24 mD. Nested artesian-volcanogenic basin (AVB) includes water-bearing complex of water-glacial formations: Holocene alluvial deposits, Upper Pleistocene-Holocene marine and alluvial-marine horizons, Upper Pleistocene glacial and water-glacial complex, water-bearing Holocene proluvial and deluvial-proluvial complex. According to the well testing data of the Bystrinsky groundwater reservoir, the permeability range is from 10 to 3000 mD. Koryaksky and Avachinsky volcanoes (Q_{3-4}) composed of andesibasalts and basalts form the water recharge area of the volcanogenic basin (Kiryukhin, Kiryukhin and Manukhin, 2010).

In terms of the gas composition, the basement fluids of the volcanic structures (except for the northern slope of Koryaksky volcano) are characterized by the ubiquitous distribution of methane (about 70 vol.% of NCG) found in the wells of the Ketkinsky geothermal field, along the southeastern periphery of the Pinachevo extrusive massif (well GK1, Pinachevo springs), southwest of the Koryaksky volcano (well E1), and wells in the Radyginsky area (well R3).

Magmatic activity in the southwestern sector of the Koryaksky volcano is manifested in the form of magma injections (magma fracking) at depths from −5.5 to −3.0 km at its southwestern foot within a radius of 1.5–4.0 km from the summit (July 2008-January 2009). The magma fracking was accompanied by formation of inclined dikes of various spreading with dip angles of 20–80° Additional Frac-Digger (Kiryukhin and Kiryukhin, 2016) analysis of magma injections from 01.2000 to 10.2019 with the search parameters ($\delta_t \leq 30$ days, $\delta_R \leq 6$ km, $\delta_Z \leq 0.2$ km, $N \geq 6$) shows also (Figs. 1 and 2) the presence of three flat dikes/sills with dip angles from 13 to 24° at the depths from −4.6 to −3.8 km (time of their injection August - November 2008). The apparent length in the section is up to 4 km (sill #49). The dip azimuth of these sills is oriented in the NE direction, which means that thermal-permeability faults may form on their continuation towards the Ketkinsky productive geothermal reservoir, provided by magmatic activity of the Koryaksky volcano (Kiryukhin et al., 2021).

Natural groundwater discharges with anomalous water salinity in the area of the Ketkinsky geothermal field - Zelenovskoye lakes are noted in the report Maltseva et al. (2011). Geophysical work carried out in 1982 (Zadirey, 1984) and electrical prospecting by ZSB method (probing by field formation in the near field) carried out in 1984 (Nurmukhamedov and Netesov, 1984; Netesov, 1989; Nurmakhamedov, 1989) were of particular importance for the organization of exploration work. One of the isolated high conductivity 13 to 20 Ohm-m column-shaped geophysical anomalies in the Zelenovsky Lakes area was explored by drilling in 1986. Well 23, 341 m deep, brought thermal waters to the surface (self-discharging flow rate of 9.3 l/s, water temperature at the wellhead of 57 °C, overpressure under flowing conditions of 0.73 bar).

2. Development of a 3D digital geological model of a productive geothermal reservoir

2.1. Three-dimensional distribution of temperature, fluid pressure, partial pressure of CH_4 and water salinity (according to measurements in wells)

To calculate the 3D temperature distribution (on a regular grid with a step of 100 m) in a geothermal reservoir, the algorithm of the universal kriging with a linear trend and a linear variogram (3D spline algorithm) is used. Numerical solution is carried out using the GREEN package from the LIDA-3 program library for function approximation and digital filtering developed at the Computer Center of the Siberian Branch of the RAS. Initial data for temperature calculations include 133 measurement points in 26 wells (Maltseva et al., 2011) as recovered bottomhole temperatures after drilling. When determining the coordinates of temperature measurement points, deviations of K4A and K8 wells from the vertical were taken into account. Temperature distributions at −1500 m and in vertical sections AB and CD are shown in Fig. 3.

The data on gas content in the producing wells and chemical analyses of their gas composition (Maltseva et al., 2011) were used to estimate

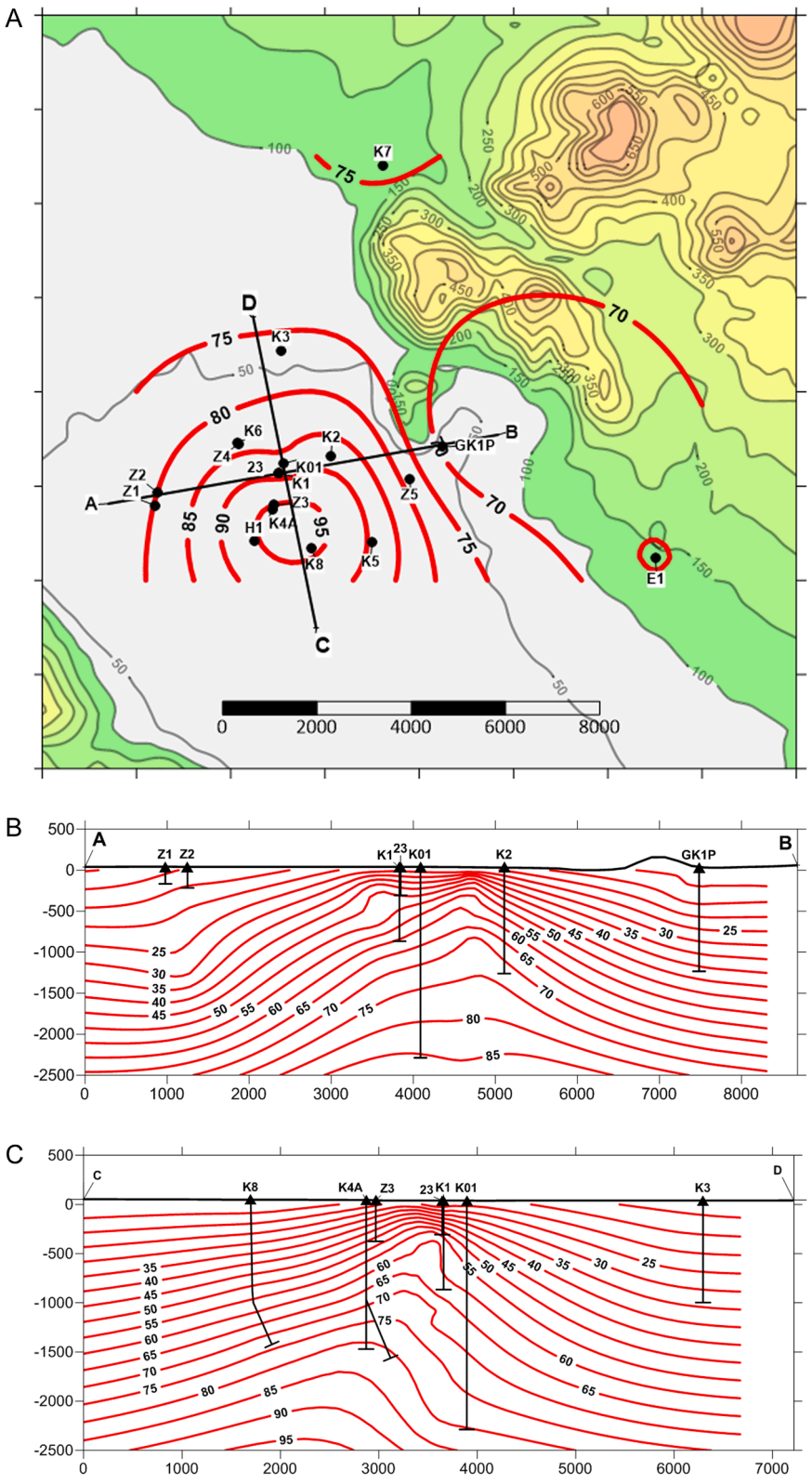

Fig. 3A Calculated temperature distribution at −2500 m shown by red lines. Topo contours are filled, marking of axes 2000 m.
Fig. 3B Calculated temperature distribution in the cross-section along the AB line (see Fig. 3A).
Fig. 3C Calculated temperature distribution in the cross-section along the CD line (see Fig. 3A).

the mass fraction and partial pressure of NCG (non condensable gasses). The results of calculations of the mass fraction and partial pressure of CH_4 for wells of the Ketkinsky geothermal field are given in Table 1. The partial pressure of non-condensable gasses was calculated according to Henry's law for methane, since CH_4 is the dominant gas and, at the same time, the least soluble.

No downhole pressure logging measurements have been performed. So reservoir pressure data were computed from surface values, with

Table 1
Calculations of mass fraction X_{CH4} and partial pressure of CH_4 in wells of Ketkinsky geothermal field. F - gas factor (l/kg), KH - Henry's constant (dependence of KH on temperature is taken from http://www.consultant.ru/document/cons_doc_LAW_317,602/67498de708a7778bac984efc34c4827fec1ecb5e/), PCH_4 was calculated in proportion to the volume fraction of CH_4 in the gas composition, in the absence of data the volume fraction was assumed to be 0.73 (73%) in vol.%. Gas composition from (Maltseva et al., 2011).

Well	He	H_2	O_2	N_2	CH_4	CO_2	Ar	F l/kg	F max	X_{CH4}	T°C well head	KH CH_4 MPa	P CH_4 bar
Z2													
K1	0.03	0.001	0	33.9	65.2	0	0.09						
K4	0.027	.0008	0.5	27.3	71.4	0.55	0.2	0.59	0.59	0.00047	57.7	6320.0	21.4
K5	0.036	0.347	0	28.9	69.9	0.04	0.08	0.253–0.455	0.455	0.00037	45.5	5468.3	13.97
K2	0.031	0.06	0	21.8	78	0.01	0.09	0.57	0.57	0.00046	48.0	5642.8	20.17
GK1	0.029	.0002	0	30.9	78.7	0.24	0.13						
23	0.022	0.067	0.2	26.4	73.1	0	0.16	0.2–0.38	0.38	0.00031	57.1	6278.1	14.01
Z3								0.27	0.27	0.00022	34.4	4693.4	7.43
Z5								0.54	0.54	0.00043	24.0	3967.4	12.57
K4A								0.85	0.85	0.00068	72.7	7367.1	36.73
K6								0.34	0.34	0.00027	55.0	6131.5	12.23
K8								0.408–0.663	0.663	0.00053	62.5	6655.0	25.88
K01								0.23–0.611	0.611	0.00049	66.0	6899.4	24.73

possible inaccuracies. Fluid pressure values were calculated using data from the Ketkinsky geothermal field well catalog as follows: (1) the depth at which the pressure was calculated was selected as the average value of the depths of the productive feed-zones, penetrated by the well and located in the intervals of perforation of the filter columns (the exception is well E-1, where the pressure calculation depth and static level were determined as the actual values at present); (2) the pressure P was calculated at the above depth from the static well level by hydrostatic law, taking into account the water density ρ(T,M) dependence on temperature T (the temperature calculated on a regular grid by spline approximation (see above)) and the salinity M of the water in the well were used:

$$\boldsymbol{P} = \int_{Z0}^{Z} \boldsymbol{\rho}(\boldsymbol{T},\boldsymbol{M})\cdot\boldsymbol{g}\cdot\boldsymbol{dZ} + \boldsymbol{P_{atm}} \quad (1)$$

- where g is gravity acceleration 9.81 m/s^2, Z0 is static level, Z is the elevation at which the fluid pressure was calculated, P_{atm} is atmospheric pressure (1 bar). TOUGH2 (Pruess et al. (1999, 2011) approximation of IFC-1967 tables was used to account for water density dependence on temperature. Linear dependence for sodium chloride brines (Shymanovich and Yasoveyev, 1989) was used to account for water density dependence on salinity. In addition, in determining the coordinates of pressure measuring points, deviations of wells K4A and K8 from the vertical were taken into account. The results of calculations of fluid pressure in Ketkinsky geothermal field wells at corresponding depths are given in Table 2.

The input data for calculating 3D fluid pressure distributions include 17 pressure values in 17 wells, input data for X_{CH4} and P_{CH4} distributions include 14 calculated values in 14 wells, and input data for thermal water salinity includes 16 values in 16 wells (Table 2). Calculations of 3D distributions were performed on a regular grid with a step of 250 m in the horizontal plane and 100 m in the vertical direction, using the 3D spline algorithm (see above).

The temperature distribution reflects the spatial properties of the productive geothermal reservoir containing a column-shaped up-flow of the deep thermal water ("thermal column", Maltseva et al., 2011), characterized by a 1200 m south-south-eastern shift in the center of the thermal anomaly, while deepening by 1500 m (dip angle about 50°). The cross-sectional area of the thermal anomaly above the 70 °C isotherm at a depth of −1500 m is about 5.3 km^2, cross section diameter of 2.6 km (Fig. 3).

The fluid pressure distribution reflects a regional pressure gradient of 0.6 bar/km (directed from NE, from the Koryaksky volcano side) and does not explicitly record a positive pressure anomaly of the thermal water up-flow (Fig. 4). The absence of a pronounced fluid pressure anomaly in the axial part of the ascending up-flow may be due to the following reasons: (1) pressure drop due to operation that began in 1986 and (or) the influence of the area of natural discharge (Zelenovskie Ozerki); (2) the two-phase state of the thermal fluids (methane in the free phase and its partial pressure higher than the calculated (Table 2)), which was not considered in calculations of fluid pressure by the formula (1).

Isolines of CH_4 mass concentrations are nonclosed and may point to

Table 2
Results of calculations of fluid pressure P (bar), mass fraction of CH_4 and partial P_{CH4} pressure, data on salinity M (g/l) in wells of Ketkinsky geothermal field. Calculation methodology is presented in the text. Notes: H stat - static level (m), Z - elevations of calculated pressure points (m).

Well	Elevation (m asl)	H stat (m)	Z (m asl)	P bar	X_{CH4}	P_{CH4} (bar)	M (g/l)
23	34.4	7.3	−268	31.513	0.00031	14.010	8.60
K01	34.2	15.7	−1524	154.783	0.00049	24.729	10.70
K6	37.8	0.27	−1282	130.336	0.00027	12.229	3.90
K4A	29.9	12.95	−1451	147.396	0.00068	36.734	11.10
K8	23.8	13.13	−1411	143.469	0.00053	25.883	10.90
K1	34	7	−691	72.822			10.40
K2	33.8	5.2	−889	92.271	0.00046	20.170	9.50
K5	21.25	7.2	−1229	125.174	0.00037	13.971	10.40
Z3	29.9	2.24	−277	31.522	0.00022	7.434	5.30
Z4	37.8	1.3	−332	37.573	0.000	0.000	2.40
H1	28.8	0.2	−306	33.983	0.000	0.000	
Z5	28	7.7	−432	47.157	0.00043	12.567	3.90
K7	80	−2.38	−1165	123.279	0.000	0.000	2.10
Z1	36.02	−0.12	−125	16.863	0.000	0.000	0.12
GK1P	28	14.2	−448	49.403			3.80
E1	140.2	26	−492.8	60.777			0.80
Z2	36.5	1.2	−175	21.968	0.000	0.000	0.20

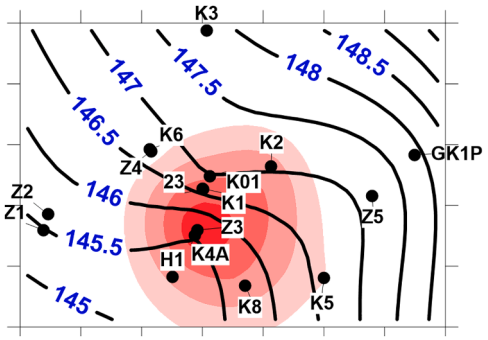

Fig. 4. Calculated fluid pressure distribution isolines (bar) at −1450 m. The background fill shows the temperature above 65 °C at the same elevation. Marking of axes 1 km.

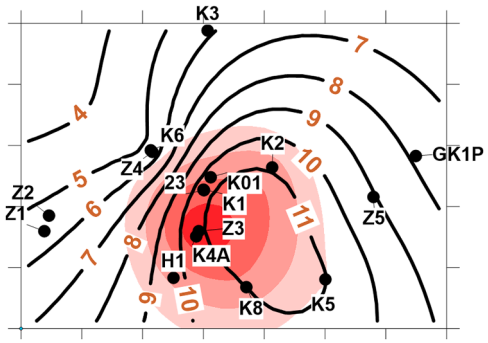

Fig. 6. Calculated distribution of salinity isolines (g/l) at −1450 m. The background fill shows the temperature above 65 °C at the same elevation. Marking of axes 1 km.

areas of thermogenic CH_4 generation, which are characterized by NE (in the lower parts of the section) or latitudinal (in the upper parts of the section) strike (Fig. 5).

The distribution of salinity is characterized by closed anomalies coincide with temperature anomalies (Fig. 6).

2.2. Identification of productive faults by 3D distribution of production feed-zones

To identify productive faults, the program Frac-Digger2 (Kiryukhin and Kiryukhin, 2017) is used, which allows identifying production faults, or plane-oriented clusters of production feed-zones of wells. The following criteria are used to select elements of plane-oriented clusters: 1) Proximity in horizontal plane $\boldsymbol{\delta_R}$; 2) Proximity to plane orientation $\boldsymbol{\delta_Z}$ (distance between sample element and plane); and 3) Minimum number of elements in a plane-oriented cluster **N**.

In the FRAC-Digger2 program, sampling from the set of points in the 3D domain is performed randomly (using the Monte Carlo method). This allows to avoid dependence of the solution on the ordering of the initial set of points, which is extremely important for 3D analysis of production feed-zones distribution and identification of productive faults. When searching for K elements from a list consisting of N elements, the maximum number of unique generations C_N^K is limited by the iteration time, so several program runs are performed to confirm the validity of the detected productive faults.

During calculations of productive faults of Ketkinsky geothermal field the following calculation parameters were accepted: δ_R=4 km, δ_Z=100 m (50 m), $N = 6$. Depths of production feed-zones top were used as initial data set (according to Ketkinsky geothermal field well catalog, taking into account deviation of wells 4A and 8), 87 zones in total were used.

As a result, three productive faults were identified, their characteristics are given in Table 3. Fig. 7 shows their 3D distribution.

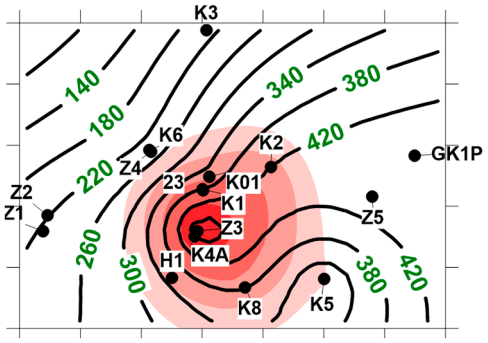

Fig. 5. Calculated distribution of CH_4 mass concentration isolines (ppm) at −1450 m The background fill shows the temperature above 65 °C at the same elevation. Marking of axes 1 km.

Local structural-tectonic map of Ketkinsky area (Netesov, 1989) shows the following regional fault systems: (1) NW striking deep faults, delineated by gravitational steps and J_3-K_2 outcrops, and NW striking neotectonic faults; (2) Sub-latitudinal faults (Malkinsky-Petropavlovsky fault zone); (3) Sub-meridional faults (Paratunsky-Asachinsky graben strike); (4) Pinachevsky extrusions array structure (that is indeed cover all drilled area and continues to NNE).

Production fault #1 is NW striking parallel to faults (1) above mentioned.

Production faults #2 and #3 are striking in NNE and NE directions, that is not coincide to strike of any regional faults systems (1, 2, 3) above mentioned. But production faults #2 and #3 are located within Pinachevsky extrusions array structure (4), that is indeed a magma fracking system with unknown fracs geometry distributions. We believe our estimates of production faults are matches to magma fracking system geometry.

2.3. Interpretation of dependence of specific flow rate of productive wells on well head pressure decline, evaluation of productivity indexes of producing wells

Tests of productive wells at the Ketkinsky geothermal field demonstrated a decrease in specific well flow rates with increasing well head pressure drop (Maltseva et al., 2011). Let us consider this issue taking into account the significant gas content (CH_4) of productive wells. The gas factor of the wells is estimated from 0.27 to 0.85 l/kg, the dominant gas is CH_4 (average volume gas content 0.73 (Table 1). When well head pressure (or water level, if pumping) in productive wells decreases, pressure in bottom hole zone decreases, and, taking into account high gas content, it may be accompanied by boiling in near-wellbore zone of the reservoir. Therefore, for interpretation of flow tests at different stages of drawdown it is necessary to use productivity indices PI_0 (m^3 or D•m) taking into account relative permeability of liquid phase (water).

In this case, the mass flow rate q of fluid phase β of the discharging wells (wells on deliverability) is determined at a bottom hole pressure P_{wb}, fluid phase pressure in the reservoir $P_\beta > P_{wb}$ and productivity index PI_0 (Pruess et al., 1999) with the following:

$$q_\beta = \frac{k_{r\beta}}{\mu_\beta}\rho_\beta \cdot PI_0 \cdot (P_\beta - P_{wb}) \quad (2)$$

-where $k_{r\beta}$, ρ_β, μ_β are relative permeability, density and viscosity of the fluid phase β, respectively. In the case of thermal water pumping, the fluid phase is liquid water and to determine its relative permeability we can use the Grant functions appropriate for productive reservoirs with fractured permeability: relative water permeability $k_{rl}(S_g) = \hat{S}^4$, where $\hat{S} = (S_l - S_{lr})/(1 - S_{lr} - S_{gr})$, in this expression S_l - is the saturation of the liquid phase, S_{lr} - is the residual water saturation, S_{gr} - is the residual saturation of the gas phase (CH_4).

Table 3
Calculated (FRAC-Digger2) characteristics of productive faults of Ketkinsky geothermal field (δ_R=4 km, δ_Z=100 m, N = 6, run 20). X, Y, Z - coordinates of the productive fault center (m).

Production fault ##	Deep angle (deg)	Azimuth angle (deg)	X m	Y m	Z m	Number of feed-zones	Fault area km^2	Total rate kg/s
1	76.0	38.1	57,077	106,262	−641	39	1.76	60.5
2	77.0	109.8	56,910	105,762	−553	19	0.49	43.3
3	24.3	139.1	56,533	105,909	−679	10	3.95	17.9

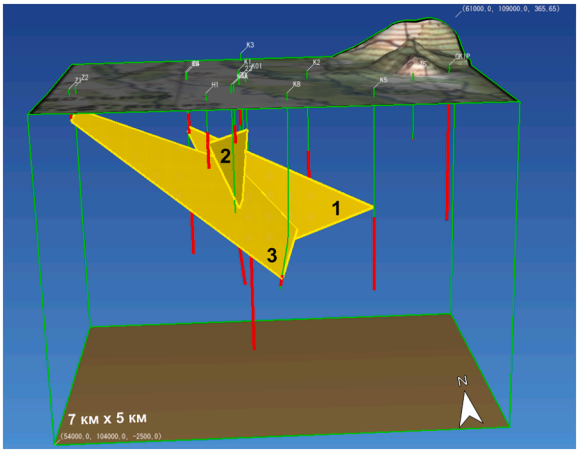

Fig. 7. 3D image of productive faults 1, 2 and 3 (Table 3).

Calculations of productivity index PI_0 (m^3) of wells according to the formula (2) were carried out according to the following algorithm: (a) Determination of flow rates q was carried out using the catalog of wells of Ketkinsky geothermal field (Maltseva et al., 2011); (b) Decrease of static water level (according to the catalog) was converted into decrease of bottom hole pressure, as a result, the value (P_β-P_{wb}) in formula (2) was estimated; (c) ρ_β, μ_β were estimated according to relationship of water density and viscosity on temperature, included in the TOUGH2 program; (d) relative permeability function (according to Grant) was chosen according to gas phase saturation value S_g so that productivity index remained close to its value determined for single-phase conditions (at minimum level drop).Thus, two-phase Grant RP PI model (Eq. (2)) shows good linear fit of the flowrate-pressure drop relationship with S_g (gas saturation) as a fitting parameter (Table 4).

Two-phase model used for Production Indexes (PI) estimations was also verified in wells, where bubbling conditions are required for linear rate vs level drawdown relationship (Table 4), e.g. wells 23, Z3, K8, K6, K4A and K01. Matches upper feed zones pressures versus partial CH_4 pressures (Table 2) in wells above mentioned shows the following: (1) Wells 23 and Z3 are in bubbling conditions; (2) Nevertheless, wells K8,

Table 4
Calculation of productivity indexes of Ketkinsky geothermal field wells. Legend: # - well number, S m – water level drop, m; Q - water phase flow rate, kg/s; T - wellhead discharge temperature, °C; Sg - estimated gas phase saturation; F - gas factor, l/kg; μ - water viscosity, Pa•s; ρ - water density, kg/m^3; PI_0 - productivity index, m^3, calculated by selecting Sg value.

#	Data	S m	Q kg/s	T°C	Sg	F l/kg	μ Pa•s	ρ kg/m^3	PI_0 m^3
23	13.08.90	6.5	7.0	57.1	0.00	0.38	4.864E-04	989.1	5.31E-11
23	19.08.90	22.3	16.3	58	0.09		4.795E-04	988.7	5.26E-11
23	10.12.90	30.7	20.3	57	0.12		4.871E-04	989.2	5.32E-11
K01	14.12.90	60.7	5.3	66.5	0.00		4.216E-04	984.3	3.71E-12
K01	18.02.91	76.6	3.3	73	0.16	0.61	3.850E-04	980.6	3.37E-12
K6	07.03.90	32.9	3.5	51.5	0.56		5.327E-04	991.7	1.51E-10
K6	11.03.90	53.4	4.7	52	0.58		5.283E-04	991.5	1.51E-10
K6	20.09.90	95.1	5.8	55	0.62	0.34	5.030E-04	990.1	1.44E-10
K6	13.12.90	106.8	6.2	55.5	0.62		4.990E-04	989.9	1.43E-10
K4A	18.04.89	20.0	3.8	72.7	0.00	0.85	3.866E-04	980.8	7.49E-12
K4A	27.07.90	17.1	3.1	69	0.00	0.85	4.068E-04	982.9	7.59E-12
K4A	03.08.90	42.1	4.9	71	0.12		3.956E-04	981.8	7.71E-12
K4A	03.10.90	65.4	5.8	71	0.17		3.956E-04	981.8	7.58E-12
K4A	10.12.90	65.1	6.1	73	0.17		3.850E-04	980.6	7.54E-12
K8	02.11.89	54.6	10.0	64	0.50		4.374E-04	985.6	1.30E-10
K8	13.11.89	8.9	4.9	61	0.35	0.48	4.577E-04	987.2	1.42E-10
K8	16.08.90	12.2	5.8	62.5	0.37	0.66	4.474E-04	986.4	1.36E-10
K8	16.09.90	33.0	7.7	64	0.47	0.41	4.374E-04	985.6	1.31E-10
K8	10.12.90	38.2	5.9	66	0.52	0.49	4.247E-04	984.6	1.25E-10
K1	11.09.86	6.0	2.0	54	0.00		5.112E-04	990.6	1.72E-11
K1	09.11.86	6.0	0.5	55	0.00		5.030E-04	990.1	4.32E-12
K2	25.05.87	23.0	3.3	49	0.02		5.556E-04	992.8	8.71E-12
K2	26.05.87	4.6	0.7	45	0.00		5.956E-04	994.5	9.11E-12
K5	20.06.88	9.8	6.6	41.2	0.00	0.25	6.379E-04	996.0	4.34E-11
K5	04.11.88	7.7	2.2	44.5	0.00	0.43	6.009E-04	994.7	1.73E-11
K5	13.11.88	7.7	2.2	45.5	0.00	0.46	5.904E-04	994.3	1.70E-11
Z3	20.07.87	2.7	4.0	34	0.17		7.327E-04	998.6	2.29E-10
Z3	22.07.87	15.8	20.0	34.5	0.21		7.254E-04	998.4	2.36E-10
Z3	01.08.88	1.3	4.2	34.4	0.00	0.27	7.269E-04	998.4	2.37E-10
Z4	13.11.87	0.7	2.0	29	0.00		8.130E-04	1000.1	2.32E-10
Z4	14.11.87	14.2	15.0	34	0.22		7.327E-04	998.6	2.09E-10
Z5	25.03.89	15.9	10.0	24	0.02		9.088E-04	1001.6	6.08E-11
Z5	13.04.89	6.4	4.0	24	0.00	0.54	9.088E-04	1001.6	5.72E-11
Z1	19.03.87	3.9	1.3	6	0.00		1.456E-03	1005.3	4.87E-11
Z2	23.04.87	12.2	6.2	6.5	0.00		1.435E-03	1005.2	7.24E-11
Z2	23.04.87	0.5	0.3	6.5	0.00		1.435E-03	1005.2	8.57E-11

K6, K4A and K01 are not in CH_4 bubbling conditions. Last contradiction may be explained by P_{CH4} underestimation, probably caused by CH_4 escape through open wellheads, when downhole pumping used for those wells flow tests (wells K8 (level drawdown to 54.6 m), K6 (level drawdown to 106.8 m), K4A (level drawdown to 65.4 m) and K01 (level drawdown to 76.6 m). Sampling underestimates are possible too: for example, gas/water ratio for well K2 is 0.57 L/kg in Table 2 (old sampling data) and 4.2 L/kg in Table 5 (recent sampling). Eventually, the following correction coefficients for mass fraction of CH_4 may be applied to fit bubbling conditions: for well K8 correction factor is 3.2, for well K6 is 8.7, for well K4A is 3.2 and for well K01 is 5.4. These corrections may extend area of CH_4 anomaly shown in Fig. 5, as well as increase potential CH_4 productivity of Ketkinsky geothermal field as a whole (with a factor from 3 to 8).

Another important issue is productivity thermal dependence. Fig. 8 shows dependence of productivity indexes PI_0 (m^3) on average discharge temperature at the wellhead of exploration wells. Comparison of discharge water temperature of wells with the temperature in the middle of the production interval shows that the discharge temperature is lower on average by 7 °C than the temperature in the middle of the production interval according to measurements in the wellbore. Significant temperature reduction occurs both due to heat exchange with the walls of the well (at flow rates less than 5 kg/s), temperature reduction caused by boiling of the fluid made possible by the remarkable CH_4 concentration and, possibly, due to the Joule-Thomson effect of expansion of gas phase CH_4 in the process of ascending the fluid from the productive zone to the wellhead. Therefore, the temperature at the wellhead is shown to be lower as compared to the inflow temperature from the production zones.

If we use in the analysis of dependence of productivity indices PI_0 (m^3) on temperature values according to measurements in the wellbore (Fig. 8), the positions of productive wells in the field of temperature-PI_0 (m^3 or D•m) are grouped quite logically. Wells producing from fractured metamorphic (mJ_3-K_I) and volcanogenic (N_{al}) rocks (K01, K2, K4A, K5, K6, K8) show productivity indexes from 3.5 to 147.1 D•m (average 48. 1 D•m) close to Sredny (SR1,2) and Nizhne-Paratunsky (NP) sites of Paratunka geothermal field (Kiryukhin et al., 2017a, Kiryukhin, 2020) and Mutnovsky geothermal field (Kiryukhin et al., 2018), wells producing from lateral flowing in Quaternary volcanic-sedimentary (Q_{III-IV}, νQ_{II-III}) rocks (23, Z1, Z2, Z3, Z4, Z5, H1) in general show higher productivity indexes from 48. 7 to 273.8 D•m (average 150.0 D•m).

2.4. Zoning of a geothermal field by temperature, permeability and lithology

Two structural-geological surfaces, substantiated by well drilling results and natural surface outcrops, can be most confidently identified within the field: (1) the combined roof of metamorphic Jurassic-Cretaceous ($J_3 - K_2$), volcanogenic-sedimentary and Neogene (N_{al}) and penetrated bottom of Quaternary (Q_{II-III}) volcanogenic rocks; (2) the basement of fluvioglacial upper-Quaternary deposits (fQ_{III}). On the indicated structural surfaces three funnels (former volcanic craters) are clearly seen: the first in the area of well K5 with a relative depth of ≈150 m and a diameter of ≈3 km; the second in the area of well 4A with a depth of ≈100 m and a diameter of 1.5 km, opened to the NW; the third is between wells K6 and K3, characterized by a relative depth of ≈150 m,

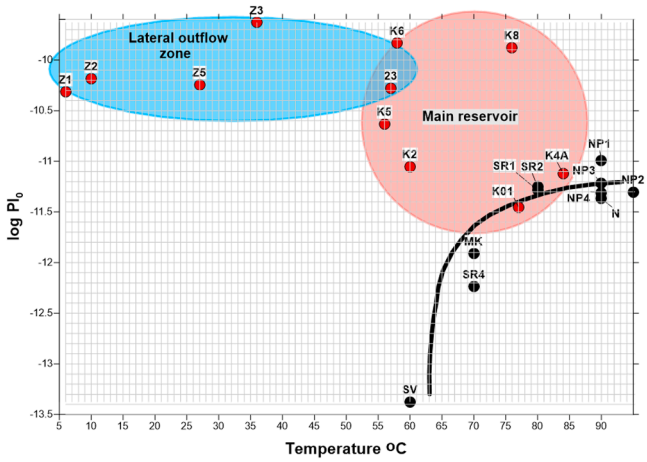

Fig. 8. Dependence of productivity indexes PI_0 (m^3) of production wells of Ketkinsky geothermal field on temperature in the middle of production interval (red circles with well numbers). For comparison, black circles show averaged productivity indices for Paratunsky geothermal field sections (Kiryukhin et al., 2017a; Kiryukhin, 2020).

elongation in the NE direction and horizontal dimensions of 3 km x 1.5 km. By analogy with the nearby Pinachevsky extrusive massif, these structural funnels can be considered as a three buried volcanic channels. In each of these channels, an active hydrothermal circulation is possible, as we can see from the data of direct temperature measurements in the boreholes on the example of the first and second structural funnels.

Based on the above information on thermal permeability and geological and structural features, the following 3D zoning of Ketkinsky geothermal field into domains (compartments, or spatial areas with similar permeability-porosity and thermal-physical properties) is used:

- RES75 domain - geothermal reservoir with temperature above 75 °C, increased permeability.
- RES55 - geothermal reservoir with temperature between 75 and 55 °C, high permeability.
- RES25 domain - geothermal reservoir with a temperature of 55 to 25 °C within the Quaternary sediments, high permeability.
- ROCK domain - Neogene (N_{al}), Jurassic-Cretaceous ($J_3 - K_2$) metamorphic, intrusive, and volcanogenic rocks with temperatures less than 55 °C, low permeability.
- domain QVOLC - Quaternary (Q_{II-III}) volcanogenic rocks with temperatures less than 25 °C, low permeability.
- domain QFLUV – fluvio-glacial upper-Quaternary deposits (fQIII) with temperature less than 25 °C, low permeability.

Fig. 9 shows corresponding 3D digital geological model of Ketkinsky geothermal field on computational grid with step $\Delta x = 250$ m, $\Delta y = 250$ m, $\Delta z = 100$ m in the depth range to −2500 m and area 7 km x 5 km.

Table 5
Gas composition (vol.%) of wells K2 and 23 of the Ketkinsky geothermal field. Samples were taken on 15.07.2020 by A.V. Kiryukhin and N.B. Zhuravlev and analyzed at the Central Chemical Laboratory of IVS FEB RAS. H_2S - was not detected.

Well	Point of sampling	T °C	He	H_2	O_2	N_2	Ar	CO_2	CH_4	C_2H_6	F l/kg
K2	Wellhead	20	0.0047	0.0002	9.91	49.34	0.46	0.16	39.91	0.21	
K2	Cap. tube	20	0.0290	0.0001	0.26	21.33	0.11	0.22	77.71	0.34	4.2
23	Gas separator	60	0.0060	0.2507	5.73	75.26	0.80	0.09	17.84	0.03	
23	Cap. tube	60	0.0277	0.0003	0.71	31.19	0.31	0.06	67.64	0.06	0.04

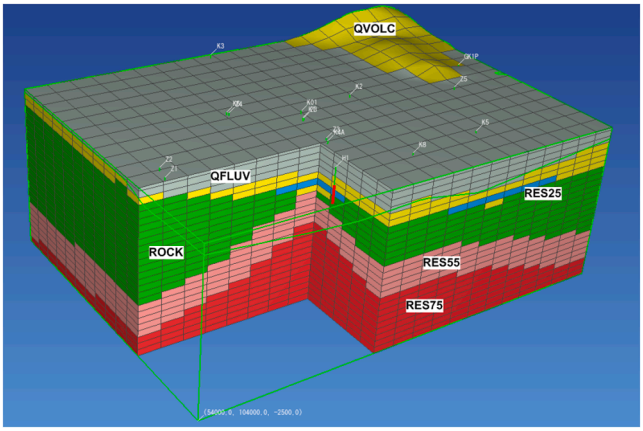

Fig. 9. 3D digital geological model of the Ketkinsky geothermal field with a notch in the SW part.

2.5. Conditions of Ketkinsky geothermal field formation according to macro-chemical, gas and isotope composition data (δD, $\delta^{18}O$)

The sampling intervals of deep wells, which penetrated the basement of the Koryaksky-Avachinsky basin (K_2, ~~P_3~~—N_1) are characterized by the chemical composition corresponding to the dilution of oceanic sedimentation water due to meteoric water infiltration. These are Cl-Na waters with insignificant contents of HCO_3, Ca, Mg, and SO_4. The Cl/Na ratio is close to seawater values, no signs of significant water-rock interaction of water are noted. Some increase in Ca and Mg may be associated with the processes of CO_2 leaching from the host rocks.

The available data on the isotopic composition of water (δD, $\delta^{18}O$) (Kiryukhin et al., 2017b) show a wide range from magmatic water (wells K01 and K5) to meteoric water (K6, Z5) with the feeding area at 1500 to 2500 m (the Pinachevsky Extrusive Massif, Arik, Aag, and Koryaksky volcanoes).

In terms of gas composition, the basement fluids of the volcanic basement (except for the northern slope of Koryaksky volcano) are characterized by the ubiquitous distribution of methane (about 70 vol. %), found in wells of the Ketkinsky geothermal field and along the southeastern periphery of the Pinachevo extrusive massif (well GK1, Pinachevo Springs) and southwest of Koryaksky volcano (well E1).

According to carbon isotopic composition $\delta^{13}C$ in free gas samples (Kiryukhin et al., 2017b), methane from Ketkinsky geothermal field wells is characterized by a sample from well K1, $\delta^{13}C=-34$ ‰ (CH_4), $\delta^{13}C=-27.7$‰ (CO_2). Judging by $\delta^{13}C$ values in methane, methane in well K1 is most likely of thermogenic origin (hydrothermal circulation in rocks containing organic matter of different origin) (Etiope et al., 2013). Nevertheless, the low $\delta^{13}C(CO_2)$ values (−27.7‰) in the methane wells indicate that a significant fraction of CO_2 here is of non-magmatic origin, and is paragenetically related to methane. According to the N_2/Ar ratio, the nitrogen in the gas composition is not of meteoric, but rather of crustal origin. Generation of hydrogen sulfide H_2S may occur by the mechanism of sulfate reduction when hydrogen H_2 enters (Zippa, 2020). But these considerations, of course, need additional justification, because they are based on sampling of well K1 only.

Based on the information presented above, Ketkinsky gas-reach geothermal field is formed by deep fluid circulation, confined to the vents of extinct volcanoes, manifested as funnels on the structural-geological surfaces and thermally conducting thermal water upflow dome, with the axis dipping to the SSW at an angle of about 50°. Paleo-injections of magma from volcanic apparatuses of Aric and Koryaksky volcanoes with subsequent magma accumulation in channel-vent systems of the Pinachevsky extrusive massif and in the Ketkinsky field basements as well as a heat mining from host rocks during deep fluids circulation are most likely are sources of thermal supply. Judging by the isotopic composition of water from productive wells, the main water recharge is also provided from the structures of Koryaksky and Arik volcanoes. The distance of 23 km between the volcanoes and the Ketkinsky geothermal field does not exclude such a possibility.

Additional data for 2020 on the chemical and gas composition of wells 23 and K2 are presented in Tables 5 and 6 and indicate a possible SiO_2-geothermometer temperature of 107 °C at depths. Even higher temperatures up to 150 °C are predicted by geothermometers in the work of Taran et al. (2021).

3. 3D digital hydrogeological model of a productive geothermal reservoir setup

3.1. Grid generation

The model was assembled using PetraSim v. 5.2 and TOUGH2-EWASG (Battistelli et al., 1997; Pruess et al., 1999). The EWASG state module describes a three-component fluid (H_2O, CH_4, NaCl) with three possible phase states (l-liquid, g-gas, s-solid).

Noting, EWASG module is enable to describe just one gas component, thus we selected the prevailing one. This is CH_4. As alternative EOS7C module can be used. EOS7C is a TOUGH2 module for multicomponent gas mixtures in the systems methane-carbon dioxide (CH_4—CO_2) or methane-nitrogen (CH_4—N_2) with or without an aqueous phase and H_2O vapor. EOS7C uses a cubic equation of state and an accurate solubility formulation along with a multiphase Darcy's Law to model flow and transport of gas and aqueous phase mixtures over a wide range of pressures and temperatures appropriate to natural gas reservoirs. Really, Henry a constant of nitrogen varies from 670 to 1100 MPa (in a range of temperatures from 20 to 100 °C), while Kh of methane is in a range from 5500 to 7500 MPa (Table 1). Thus, we can neglect more soluble gas component (N_2) in a favor of less one (CH_4) in two-phase flows considerations.

The computational grid is defined in a volume, the top of which is the topographic surface of the Earth, the bottom of which is −2500 m; the boundaries in the horizontal plane $x = [54000, 61000]$, $y = [104000, 109000]$). When generating computational grid below 0 m we used regular step $\Delta x = 250$ m, $\Delta y = 250$ m, $\Delta z = 100$ m; above 0 m we used layer with variable thickness equal to topographic height. Respectively the centers of model elements (below 0 m) are located in points with coordinates $x_i=54125+250\bullet I$, $i = 1,28$; $y_j=104125+250\bullet j$, $j = 1,20$; $z_k=-2450+100\bullet k$, $k = 1,25$. Elements of the model above 0 m are located at points with the same coordinates x,y and with coordinate z equal to half of the topographic elevation at the corresponding point x,y. A total of 14,560 elements are defined in the model.

3.2. Temperature and pressure initialization in the model

Initial conditions for temperature and pressure in model elements (INCON file) were determined by 3D spline approximation of actual data (see Section 2.1) at points with coordinates in the centers of model elements (see above). In the upper layer of the model (above 0 m) fixed values of temperature equal to 10°C and pressure 1 bar were set.

3.3. Determination of (permeability, porosity, compressibility) and petrophysical (density, thermal conductivity, specific heat) properties in the model elements

The model was zoned into domains with different permeability properties according to the principle outlined in Section 2.4, i.e., eight domains with different permeability and petrophysical properties were identified: (1) RES70 domain - geothermal reservoir with temperature above 70 °C, increased permeability; (2) RES55 domain - geothermal reservoir with temperature from 70 to 55 °C, increased permeability; (3) RES25 domain - geothermal reservoir with temperature from 55 to 25 °C within quaternary deposits, high permeability; (4) ROCK domain -

Table 6
Chemical composition of wells K2 and 23 of the Ketkinsky geothermal field. Samples were taken on 15.07.2020 by A.V. Kiryukhin and N.B. Zhuravlev and analyzed at the Central Chemical Laboratory of IVS FEB RAS. Fe2+, Fe3+ less than 0.1 ppm.

Well	pH	HCO_3^-	CO_3^{2-}	Cl-	SO_4^{--}	F	Li^+	Na^+	K^+	Ca^{2+}	Mg^{2+}	NH_4^+	H_3BO_3	SiO_2	T Na-K	T SiO_2	M ppm
K2	6.0	13	–	4752	41	0.9	1.5	2514	67	510	2	8	103	56	79	107	8073
23	8.4	43	5.4	4752	5	1.3	1.6	2417	67	441	3	10	101	47	81	99	7892

Neogene (N_{al}), Jurassic-Cretaceous (J_3 to K_2) metamorphic, intrusive, and volcanogenic rocks with temperatures less than 55 °C, low permeability; (5) domain QVOLC - quaternary (Q_{II-III}) volcanogenic rocks with temperature less than 25°C; (6) domain QFLUV - fluvioglacial upper-quaternary deposits (fQ_{III}) with temperature less than 25°C. In addition, at the base of the model the region of the deep recharge inflow (domain (7) UPFLO) is defined. The UPFLO domain is defined as the projection of the 70°C isotherm at −1550 m to the model base −2450 m The domain (8) DISCH (with Dirichlet conditions (Fixed State)) was defined in the discharge area (Zelenovskoe Lakes area). Table 7 and Fig. 10 shows the characteristics of the domains specified above. The host rock domains (ROCK, QFLUV, QVOLC) are given low permeability.

3.4. Determination on the model of sources (zones of thermal waters upflows) and sinks (discharge and ground water infiltration areas)

In the region of the thermal water upflows (UPFLO domain), defined as the projection of the 70 °C isotherm at −1550 m onto the model base −2450 m has an area $S = 9.437$ km^2, in this region the mass flux of water q, methane q_{CH4}, and NaCl q_{NaCl} is assigned as an initial approximation. Thus, the mass rates of water, methane and NaCl at the base of the model are S•q, respectively.

The discharge area is defined on the model in the upper layer above the elevation of 0 m, and the Fixed State (Dirichlet boundary conditions) are defined in it. Permeable domain DISCH, adjoins this layer from below.

Fig. 10, together with Table 7, describe the 3D digital hydrogeological model of the Ketkinsky geothermal field (domains with different permeability properties and boundary conditions for discharge area and bottom upflow zone.

4. Inversion iTOUGH2 modeling of the natural thermo-hydrodynamic-chemical state

Four scenarios of inversion iTOUGH2-EWASG (Finsterle, 1999, 2014; Kiryukhin et al., 2008) modeling were performed to estimate permeabilities, upflow rates and pressures in the discharge area (specified modeling time is 100 years). To calibrate the models, the values of pressures, temperature and salinity at the centers of the model elements including wells 23, K01, K6, K4A, K8, K1, K2, K5, Z3, Z4, Z5 were used (Table 8). Recalculation to element centers was performed using the results of 3D spline approximation of initial conditions (see above). In

Table 7
Permeability-capacity and petrophysical properties (initial approximation) determined in the model domains (Model-6_NS). ρ - mineral density of rocks, kg/m^3; Φ - porosity; k - permeability mD (10^{-15}m^2); λ - thermal conductivity, W/m/°C; HC - specific heat capacity, J/kg/ °C; C - compressibility Pa^{-1}; RP - relative permeability.

Model domain	ρ kg/m^3	Φ	k, mD (10^{-15} m^2)	λ W/m/°C	HC J/kg/°C	RP (S_{lr}=0.3, S_{gr}=0.05)
RES70	2700	0.05	8	2.0	1000	Grant
RES55	2600	0.1	8	2.0	1000	Grant
RES25	2600	0.2	50	1.4	1000	Grant
ROCK	2800	0.01	0.001	2.0	1000	Corey
QVOLC	2600	0.2	0.001	1.4	1000	Corey
QFLUV	2600	0.2	0.001	1.4	1000	Corey
UPFLO	2800	0.05	8	2.0	1000	Grant
DISCH	2600	0.2	50	1.0	1000	Grant

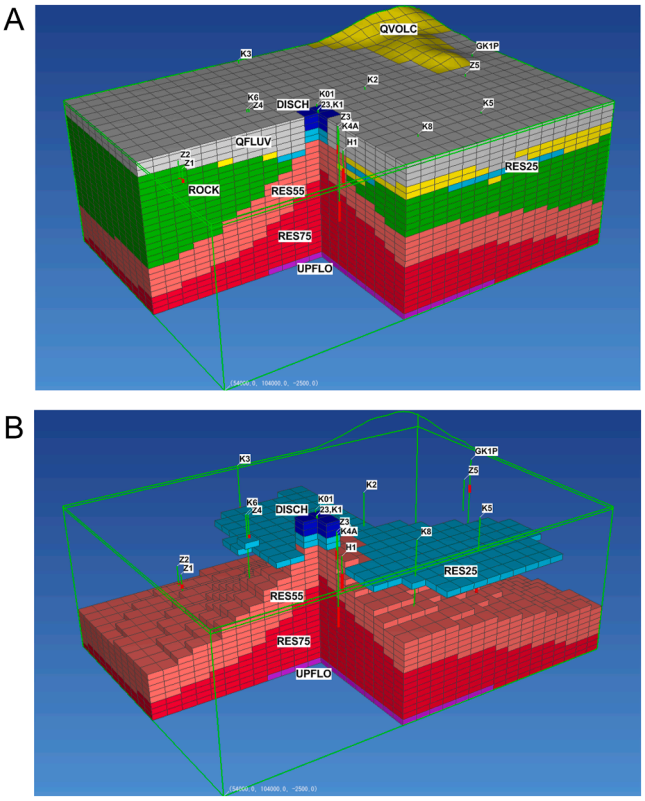

Fig. 10A 3D digital hydrogeological model of the Ketkinsky geothermal field with a notch in the SW part.
Fig. 10B 3D digital hydrogeological model of the Ketkinsky geothermal field with a notch in the SW part. The low-permeability ROCK, QVOLC and QFLUV domains are extracted on the model. Thus, the model shows the contours of Ketkinsky productive hydrothermal reservoir distribution. UPFLO-region of deep thermal water upflow, DISCH – discharge area (P_{up_bon} pressure in the outflow area at +20 m (bar) is defined as 1 bar).

Table 8
Calibration points used for inversion iTOUGH2-EWASG thermo-hydrodynamic modeling.

Well ##	Model element ##	Fluid pressure, bars	Temperature, °C	Salinity, g/kg
23	12585	29.76	52.6	8.6
K01	_5305	156.63	76.7	10.7
K6	_7037	127.18	58.7	3.9
K4A	_5780	145.56	83.2	11.1
K8	_5699	145.704	74.2	10.9
K1	10345	68.789	62.4	10.4
K2	_9257	88.510	57.6	9.5
K5	_6825	127.199	55.3	10.4
Z3	12500	29.022	34.1	5.3
Z4	12077	39.400	32.3	2.4
Z5	11448	49.236	26.6	3.9

total, 33 calibration points were used for model calibration (Table 8).

A summary of the inversion modeling results with the estimated parameters is given below.

Simulation scenario #19 (thermo-hydrodynamic simulation) reproduces the calculated pressures and temperatures at the calibration points on average (0.41 bar, −0.6 °C) and by standard deviation (0.86 bar, 2.1 °C). The permeability of the UPFLO, RES70, RES55 (deep reservoir) domains is estimated at 41.9 mD, the permeability of the RES25, DISCH (shallow reservoir) domains is estimated at 208.3 mD. The flow rate of the deep upflow (with a fixed mass fraction of CH_4 of 0.0004 and a fixed mass fraction of NaCl of 0.012) is estimated at 12.3 kg/s. The simulation also shows that the upper part of the hydrothermal reservoir with a diameter of about 500 m (to a depth of −150 m) is under natural conditions in a two-phase state (water+methane) with gas phase saturation up to 0.05. Statistical analysis of inversion modeling results (built into iTOUGH2) shows high model sensitivity to the upflow rate and reservoir permeability parameters, with their significant correlation (0.85 and 0.41).

Modeling scenario #20 (thermo-hydrodynamic-chemical simulation) reproduces the calculated pressures, temperatures and salinity at calibration points on average (0.56 bar, −0.5 °C, −0.16 g/kg) and by standard deviation (0.80 bar, 1.8 °C, 0.38 g/kg). The permeability of the UPFLO, RES70 RES55 (deep reservoir) domains is estimated at 35.3 mD, the permeability of the RES25, DISCH (shallow reservoir) domains is estimated at 190.4 mD. The flow rate of the deep upflow (with a fixed mass fraction of CH_4 of 0.0004 and a fixed mass content of NaCl of 0.012) is estimated at 9.8 kg/s. Modeling also shows that the upper part of the hydrothermal reservoir near well 23 with a diameter of about 500 m (in the depth range of −50 to −250 m) and near well K2 at −250 m is naturally in a two-phase state (water+methane) with gas phase saturation to 0. 05. Statistical analysis of the results of inversion modeling (embedded in iTOUGH2) shows high model sensitivity of the deep upflow rate and reservoir permeabilities parameters, with their correlation (0.7 and 0.6).

5. iTOUGH2 modeling of exploitation history 1986–2020

5.1. Inverse iTOUGH2 simulation of hydrodynamic exploitation history 1989–1993

The observational data used for model calibration are the data on

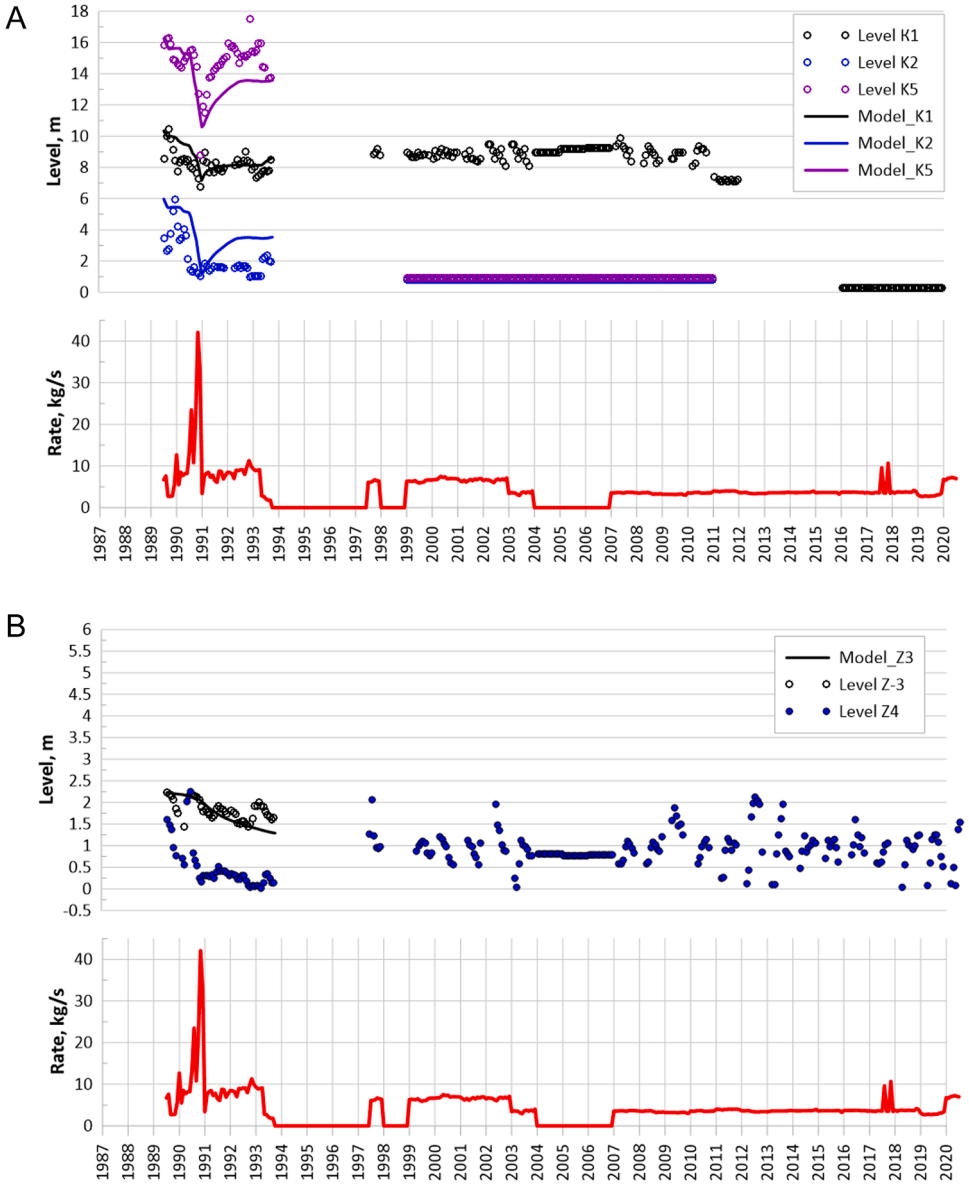

Fig. 11A Inversion modeling (scenario KM8_EX_3A) of the hydrodynamic history of Ketkinsky geothermal field exploitation (wells K1, K2, K5).
Fig. 11B Inversion modeling (scenario KM8_EX_3A) of the hydrodynamic history of Ketkinsky geothermal field exploitation (well Z3).

changes in mean monthly level in observation wells K1, K2, K5 and Z3 from 07.1989 to 10.1993 (total 193 calibration points) (Maltseva et al., 2011). Unfortunately, the data on level changes in the above observation wells for 1994–2020 are not sensitive to changes in water withdrawal rates, so using them to calibrate the model makes no sense. The compressibility of the deep reservoir (RES70, RES55, UPFLO model domains) and the compressibility of the shallow reservoir (RES25, DISCH, DISC2 model domains) were used as estimated model parameters. In this study we assumed rock porosity to be reasonable values of 0.05 for RES70, 0.1 for RES55 and 0.2 for RES25 (Table 7). If our porosity assumption is underestimate, then iTOUGH2 will overestimate compressibility. But final output of storativity is calibrated to be fit pressure drop history data. Compressibility of the host rocks (domain of model ROCK1) was taken to be 1E-8 Pa^{-1}. The >>>>SHIFT (shift) parameters (Finsterle, 2014) were also used as estimated model parameters to synchronize the starting point of the calibration data with the initial model conditions.

Scenario of inversion modeling KM8_EX_3A (Fig. 11A and 11B) is based on the results of thermohydrodynamic modeling of the natural state (variant 19, see Section 4). The resulting compressibility estimates are as follows: deep reservoir 7.16E-10 Pa^{-1}, shallow reservoir 4.14E-07 Pa^{-1}. The large difference of compressibility between deep and shallow reservoirs may be explained using Figs. 11A and 11B, where transient level responses are shown for monitoring wells in deep reservoir (wells K1, K2, K5 on Fig. 11A) and well in shallow reservoir Z3 (Fig. 11B) during multi-well flow tests/exploitation start up 1989–1993 year. One can clearly see sharp pressure drawdown features in deep reservoir (Fig. 11A), while no any such feature in shallow reservoir, just smooth pressure decline (Fig. 11B). This is a qualitative proof of high compressibility/storativity of the shallow reservoir. Statistical analysis of the results of inversion modeling (embedded in iTOUGH2) shows that both estimated model parameters are sensitive with respect to the original data, the relationship of the estimated parameters is characterized by a weak negative correlation. The discrepancies between the simulation results and the observational data are −0.02 bar (average) and 0.13 bar (standard deviation). The >>>>SHIFT parameters (Finsterle S. iTOUGH2 V7.0 Command Reference, 2014. p. 222) for wells K1, K2 and K5 are estimated at −1.0, −0.6 and −1.6 bar, respectively.

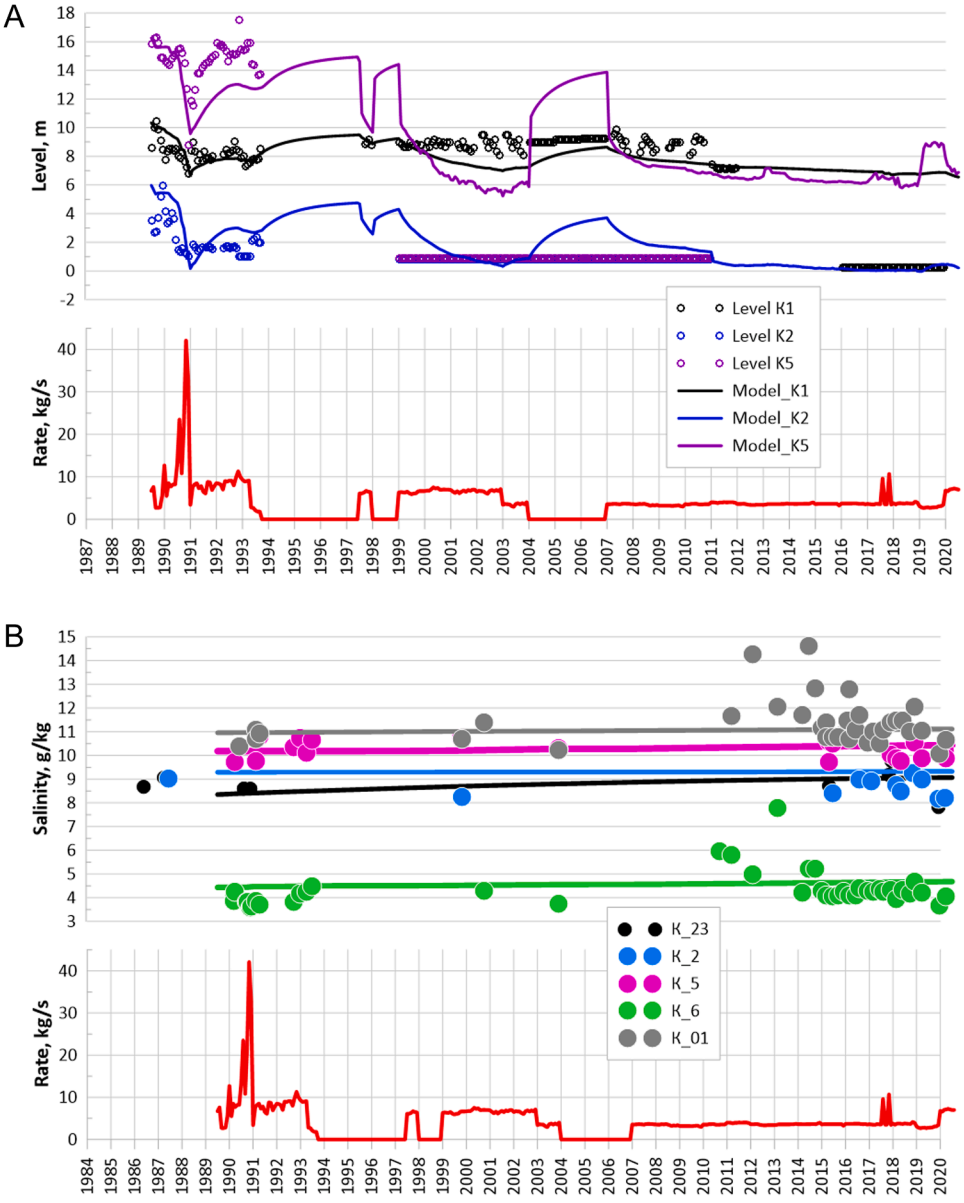

Fig. 12A Direct modeling (scenario KM8_EX_4) of the thermo-hydrodynamic-chemical exploitation history of the Ketkinsky geothermal field (levels in wells K1, K2, K5).
Fig. 12B Direct modeling (KM8_EX_4 scenario) of the thermo-hydrodynamic-chemical exploitation history of the Ketkinsky geothermal field (salinity of wells 23, K2, K5, K6, K01).

5.2. Direct iTOUGH2 modeling of thermohydrodynamic-chemical exploitation history 1989–2020

The results of direct iTOUGH2 modeling (scenario KM8_EX_4) of the thermo-hydrodynamic-chemical exploitation history of 1989–2020 (with parameters determined by the inversion modeling variant KM8_EX_3A exploittation history) are shown in Fig. 12. The results of pressure change modeling were converted to level changes using the function (>>>>SHIFT, iTOUGH2 Command Ref, 2014), for wells K2, K5, and K6 cutoffs (29.6 °C, 13.0 °C, and 6.5 °C) were also applied in the analysis of the temperature change history.

Fig. 12A shows a comparison of the results of modeling of the level regime with the actual data for wells K1, K2 and K5. With the exception of well K1, there is no correspondence between the model and actual data on the level regime for the period after 1994 or there is no actual data. Non-sensitivity of observation wells to changes in water withdrawal rates after 1994 can be caused by depressurization of their wellheads due to partial pressure of CH_4 if these wells were with the head valve closed.

Simulations show no appreciable temperature changes in wells K1, K2, K5 and K6. In this regard, we can assume that: (1) the actually observed increase in temperature in wells K6 and K01 is due to heating of the production casing during prolonged low-flow operation; (2) the decrease in temperature in well K2 is due to depressurization of the wellhead.

Changes in salinity in the wells during operation in 1987–2020 are reproduced quite well on the model (Fig. 12B), including some trend of its increase in wells 23 and K5. The 2013–2014 salinity outbursts from well K01 are not reflected in the model.

Modeling of gas-content changes in well 23 shows a steady increase from 0.002 to 0.0065 from 1989 to 2020. No regular data are available to compare the simulation results with the actual history of gas-content change during operation. A single measurement in well K2 (July 2020) shows an increase in gas content of up to 4 L/kg (Table 5), which is significantly (7 times) higher than 0.57 L/kg (Table 2, 1987 data).

Fig. 13 shows a conceptual model of pressure distribution in a completely closed observation well, penetrating water-methane reservoir. From the figure it is clear that if there is a separation of water and CH_4 in the wellbore, then methane CH_4 accumulates under the wellhead, and from the condition of hydrostatic equilibrium the following relation must be fulfilled: pressure in the reservoir = weight of water column + partial pressure of CH_4 gas cap. Hence, it follows: (1) The necessity of using in such cases the depth gauges for measuring the pressure in the reservoir (transient pressure in the process of exploitation), if the water level in such a well is not measured; (2) The increase of the wellhead pressure up to the partial pressure of CH_4 (from 7.4 to 36.7 bar, see Tables 1 and 2), which can be accompanied by depressurization and destruction of the wellhead part. The possibility of such processes is shown by the level increase in well 23 in 2019 to 25.1 m, which is higher than the initial level value of 7.63 m in 1987.

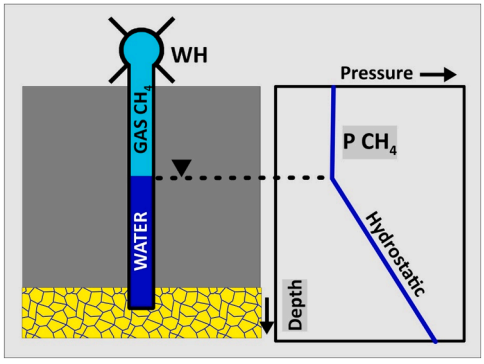

Fig. 13. Pressure distribution in a completely closed observation well, penetrating a water-methane reservoir. It is clear from the figure that if separation into water and CH_4 occurs in the wellbore, methane at partial pressure P_{CH4} accumulates under the wellhead. In this case, wellhead pressure measurements do not reflect pressure changes in the reservoir and can not be used for transient pressure analysis during flow tests, the wellhead part is at risk of failure and depressurization, if the wellhead equipment is not designed for P_{CH4} pressure (Table 1).

6. Predictive modeling in connection with the calculation of production reserves

6.1. Setting up production wells on the model

The regulation of the planned production of thermal waters at Ketkinsky geothermal field for the period of 2020–2045 is defined by the operator of the field in accordance with Table 9. At the same time it is planned to repair the existing wells K6, K01, K5, drill doublers of the existing wells 23 (1REK), K4A (2REK), K8 (3REK) and drill a new additional well 4REK to a depth of 1500 m in the position shown in Fig. 14. The expected rates of repaired wells, doublers and new additional well and their schedule for the year are also given in Table 9. The total expected well flow rate is 53.6 kg/s from 2024 to 2045.

The flow rates of production wells in the model are determined in accordance with Table 9; the production intervals of production wells are determined in the model elements corresponding to the calibration points of fluid pressure, temperature and salinity (Table 8) or the average values of the roofs of productive zones for each of the mentioned production wells. For well 4REK, the production interval was determined on the model in element _7491 (interval from −1200 to −1100 m (this interval corresponds to the intersection of productive faults 1 and 3 identified earlier, Fig. 7).

The following flow rates are assumed for the doubled wells and repaired wells; 1REK - 17 kg/s, K6A - 3.5 kg/s, K01A - 2.0 kg/s, K5A - 5.0 kg/s, 2REK - 5.0 kg/s, 3REK - 6.0 kg/s, 4REK - 15.0 kg/s.

6.2. Predictive modeling of operation with specified constant flow rates of production wells

The results of predictive modeling of operation 2020 - 2045 with the rates of production wells specified in Table 9 (Forecast_1) show the following.

Reservoir pressure drops from 1.68 bar (well 23) to 5.57 bar (well K5), in wells K8 and K4A pressure drops to 5.19 bar and 4.70 bar respectively, in wells K01, K6, K2 and 4REK reservoir pressure drops from 4.18 bar to 4.29 bar. The hydrodynamic meaning of these changes is that wells close to the discharge region (constant pressure Dirichlet boundary, cold groundwater) are characterized by the least pressure decrease (well 23), while wells far from the discharge region show the greatest pressure decrease (well K5).

The most significant temperature drop of −9.8 °C is predicted for well 23, for other production wells the predicted temperature changes are insignificant: from −0.13 °C (well K2) to +1.7 °C (well K5). The thermal meaning of these changes is that wells close to the discharge area (constant temperature Dirichlet boundary, cold groundwater) experience significant cooling (well 23), while wells far from the discharge area do not experience significant temperature changes (well K5).

Two-phase conditions in the reservoir at the beginning of the predictive modeling exist only in the production zone of well 23. Modeling shows that two-phase conditions disappear by 2031. This is the result of dilution of the shallow productive reservoir by inflow from groundwater horizons, since the planned water withdrawal rate of 53.6 kg/s exceeds the natural upflow in the productive geothermal reservoir, which is estimated from 9.8 kg/s to 12.3 kg/s.

A similar effect is observed on the predicted plots of changes in salinity. Depending on the distance from the groundwater/upflow zone

Table 9
Planned production of thermal water at Ketkinsky geothermal field in 2020–2045 (in kg/s), wells flowrates are also given in Section 6.1).

Time period, years	Wells								
	23 (1REK)	K6	K01	K5	K4A (2REK)	Z3	K2	K8 (3REK)	4REK
2020	3.28	0.89	1.46	1.24			0.12		
2021	1REK	0.89	1.46	1.24			0.12		
2022	1REK	0.89	1.46	1.24	2REK		0.12		
2023	1REK	0.89	1.46	1.24	2REK		0.12	3REK	
2024	1REK	K6A	K01A	K5A	2REK		0.12	3REK	4REK
2045	1REK	K6A	K01A	K5A	2REK	-	0.12	3REK	4REK

Notes: Well 1REK will be the standby well for well 23, planned 5–7 m from well 23; well K6A is well K6 after workover; well K01A is well K01 after workover; well K5A is well K5 after workover; well 2REK is located 5–7 m from well K-4A; well 3REK is located 5–7 m from well K8; well 4REK is located southeast K5 after workover; well 2REK is 5–7 m away from well K-4A; well 3REK is 5–7 m away from well K8; well 4REK is to the southeast of well 23 and northeast of well K-4A (see Fig. 14 for locations).

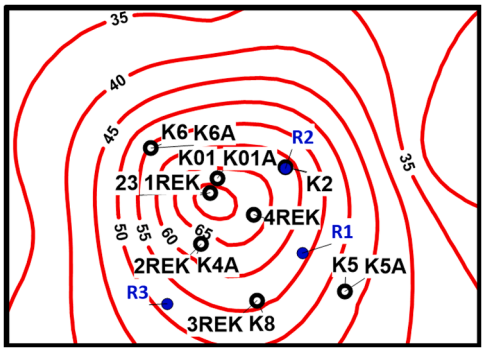

Fig. 14. The layout of production and reinjection wells, adopted in the predictive TOUGH2-EWASG modeling. Background temperature distribution at −1000 m.

to the productive reservoir and the load of production wells, salinity of production wells decreases (wells 23, K01, K4A) or increases (wells 4REK, K2, K8, K5, K6). The most significant decrease in salinity is predicted for well 23 to −4.3 g/kg, for the other production wells the predicted changes in salinity are insignificant (up to 0.3 g/kg).

Thus, the results of predictive modeling show significant pressure decreases in the deep productive reservoir (more than 4.2 bar), which obviously will prevent the operation of wells in self-discharge mode and will require the use of submersible pumps or replenishment of the water resources by the reinjection.

6.3. Predictive modeling of the operation of existing production wells using submersible pumps

In the considered variant (Forecast_6) 23, K6, K01, K5 are considered as production wells, and their operation in the "well on deliverability" mode with submersible pumps (except well 23 which is set in the self-discharge mode). As submersible pumps we consider pumps of ECV type with immersion depth of 70 m. The productivity indices chosen for modeling correspond to the data of 2020 (table 10) (note that productivity indices of wells K01, K5 and K6 have considerably (by 1 - 2 orders) lowered as compared to the initial ones (Fig. 8) due to damage of wellhead sections by partial pressure of CH_4 at valves' closing for pressure recovery). The bottom-hole pressures of the producing wells K6, K01, K5 (Table 10) were determined by means of TOUGH2-EWASG program using 1D model calculation with pump installation at the depth of 70 m (in the interval from Z_{pump}=Z_{wh} −70 m to Z_b with 1 bar pressure at Z_{pump} level) with correction (−1 bar) for water discharge/water supply area elevation it is necessary to take into account the elevations of the upper layer in the model where the discharge conditions are determined (Dirichlet BC) are set +20 m (DISC2 material), which is 10 m below the natural discharge level, therefore the model downhole pressures should be reduced by 1 bar to synchronize with the model

Table 10
Input data for forecast modeling (Forecast_6) of wells 23, K6, K01, K5 operation with submersible pumps (except for well 23) installed at the depth of 70 m for the period 2021–2045. Note: P_b (bar) - assigned bottomhole pressures of production wells, Input data for P_b calculation are: mass fraction of CH_4 (Table 2), mass fraction of Na-Cl (Xsm) (Table 2), temperature and Z_b elevations corresponding to the model element centers in Table 8, Z_{pump} - elevation of the submersible pump installation, m. Productivity indices PI_0 were estimated by formula (2), model temperature (°C) and pressure (bar) for 2020.

Model parameter	wells/model element			
	23 12585	K6 _7037	K01 _5305	K5 _6825
PI_0 m^3	1.2E-10	4.14E-12	2.18E-12	3.45E-12
X_{CH4}	0.0002	0.0002	0.0004	0.0003
X_{sm}	0.0086	0.0039	0.0107	0.0104
Z_b m	−250	−1250	−1550	−1250
Z_{pump} m	34.4	−32.2	−35.8	−48.7
P bar (model)	27.62	126.6	155.8	126.4
T °C (model)	56.9	58.8	76.8	55.9
P_b bar (assigned)	27.49	118.7	146.7	117.8

elevations of the potential water-recharge region in the course of operation). Well 23 is set in self-discharge mode (Z_{pump}=Z_{wh}).

According to the predictive modeling, during the estimated period of 25-year operation from 2021 to 2045, the temperature in production wells 23, K6, K01, K5 will increase to 1.7 °C. Total thermal water flow rate from production wells will decrease from 18.9 kg/s to 14.2 kg/s (−24.8%) (Fig. 15A), total gas component (CH_4) flow rate from production wells will decrease from 7.5 g/s to 5.7 g/s (−24%) (Fig. 15B), changes in M salinity are generally minor with M increasing for all wells. For the end-of-life period, the three deep wells with submersible pumps will have flow rates of 4.2 to 5.0 kg/s, while well 23 will reduce its capacity to 0.7 kg/s. For gas, the three deep wells with submersible pumps will have flow rates of 1.7 to 2.0 g/s CH_4, while well 23 will reduce its gas capacity to 0.3 g/s CH_4.

6.4. Predictive modeling of the operation of existing and additional production wells using submersible pumps

In addition to the previous scenario, wells K4A (2REK), K8 (3REK), K2A and a new additional well 4REK (Forecast_7) were added to the model. The modeled values of downhole pressures and productivity indices of the indicated wells correspond to the values of the initial flowtests data, see Fig. 8 and Table 11, productivity index of well 4REK is taken as an average value of productivity indices of wells K4A (2REK), K8A (3REK), K2A.

According to the forecast modeling, during estimated period of 25-year operation from 2021 to 2045 the temperature in production wells K6, K01, K5, K4A (2REK), K8A (3REK), K2A, 4REK will not change significantly (changes till +−1°C, whereas in well 23 the temperature drop 6.2°C is forecast. The total thermal water flow rate from production

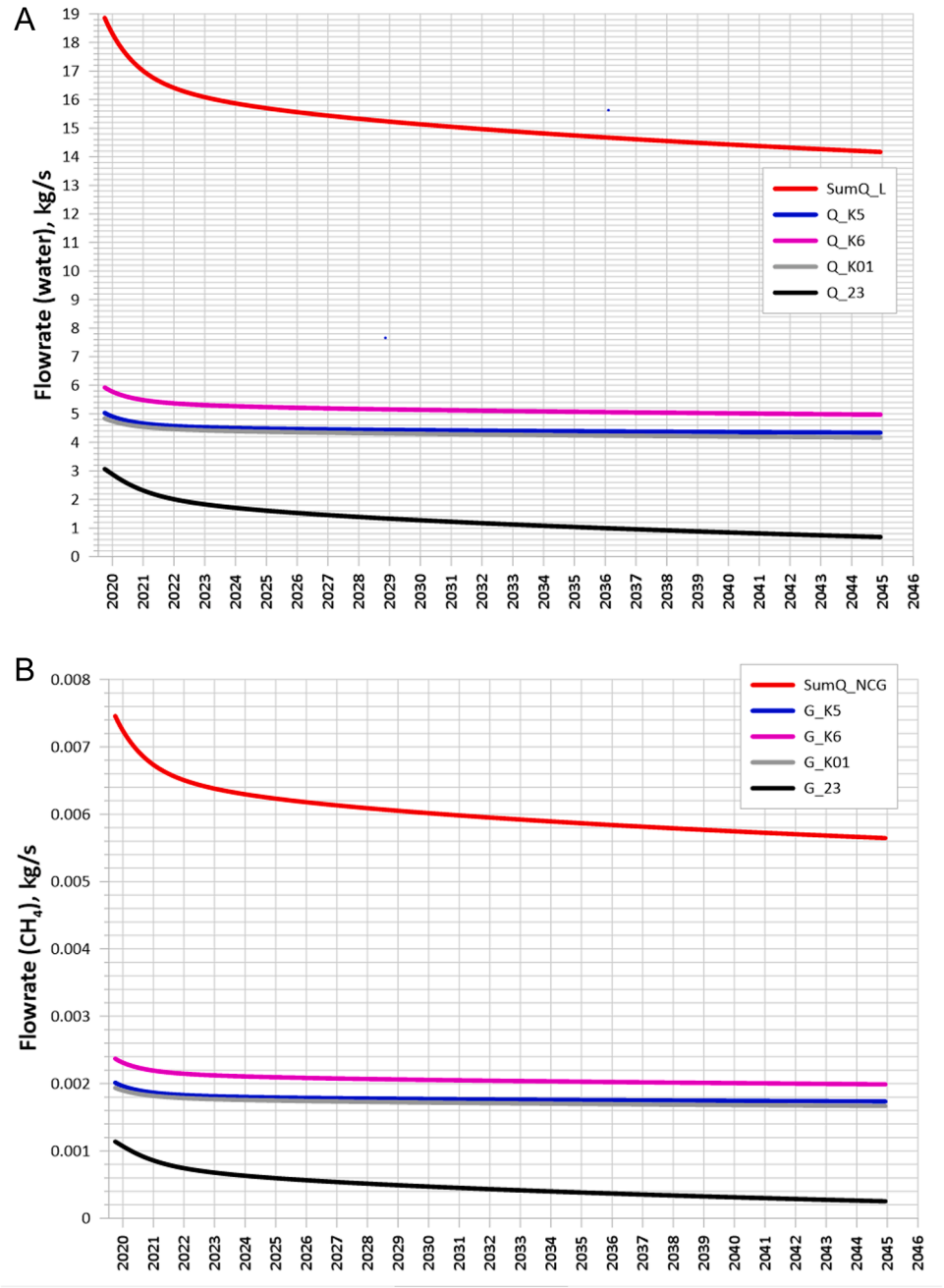

Fig. 15. **A** Forecast of changes in total and individual thermal water discharge from production wells 23, K6, K01, K5 (Forecast_6 modeling scenario).
B Forecast of changes in the total and individual rate of the gas component (CH_4) from production wells 23, K6, K01, K5 (Forecast_6 modeling scenario).

Table 11
Initial data for predictive modeling (Forecast_7) of well K4A (2REK), K8A (3REK), K2A, 4REK operation in the mode with submersible pumps installed at a depth of 70 m. Note: see note to Table 10.

Model parameter	wells/elements			
	K4A (2REK) _5780	K8 (3REK) _5699	K2A _9257	4REK _7491
PI_0 m^3	7.58E-12	1.33E-10	8.91E-12	5.0E-11
X_{CH4} (model)	0.0005	0.0004	0.0004	0.0004
Xsm (model)	0.0111	0.0109	0.0095	0.0110
Z_b m	−1450	−1450	−850	−1150
Z_{pump} m	−40.1	−46.2	−36.2	−40.0
P bar (model)	146.3	146.4	87.8	117.1
T °C (model)	83	74.2	57.3	71.6
P_b bar (assigned)	134.8	135.0	79.0	106.9

wells will decrease from the initial 151.2 kg/s to 54.3 kg/s (−64.1%) (Fig. 16A), the total gas component (CH_4) flow rate from production wells will decrease from 60.4 g/s to 21.7 g/s (−64.1%) (Fig. 16B). Wells K4A (2REK), K8A (3REK), 4REK will have the highest individual productivity from 10 to 30 kg/s each, wells K6, K01, K5, K2A will have low productivity up to 5 kg/s each, well 23 will stop discharge after 1 year of operation. Changes of salinity of M as a whole are insignificant (from −0.65 to 0.3 g/l), and decrease of M is expected for wells K01, K4A (2REK), 4REK while wells K6, K5, K8A (3REK), K2A expect slight increase of M. In well 23 the decrease of salinity is significant (−3.9 g/l). Thus, wells distant from the discharge area and characterized by high productivity indices will show the highest productivity at the end of the operation period.

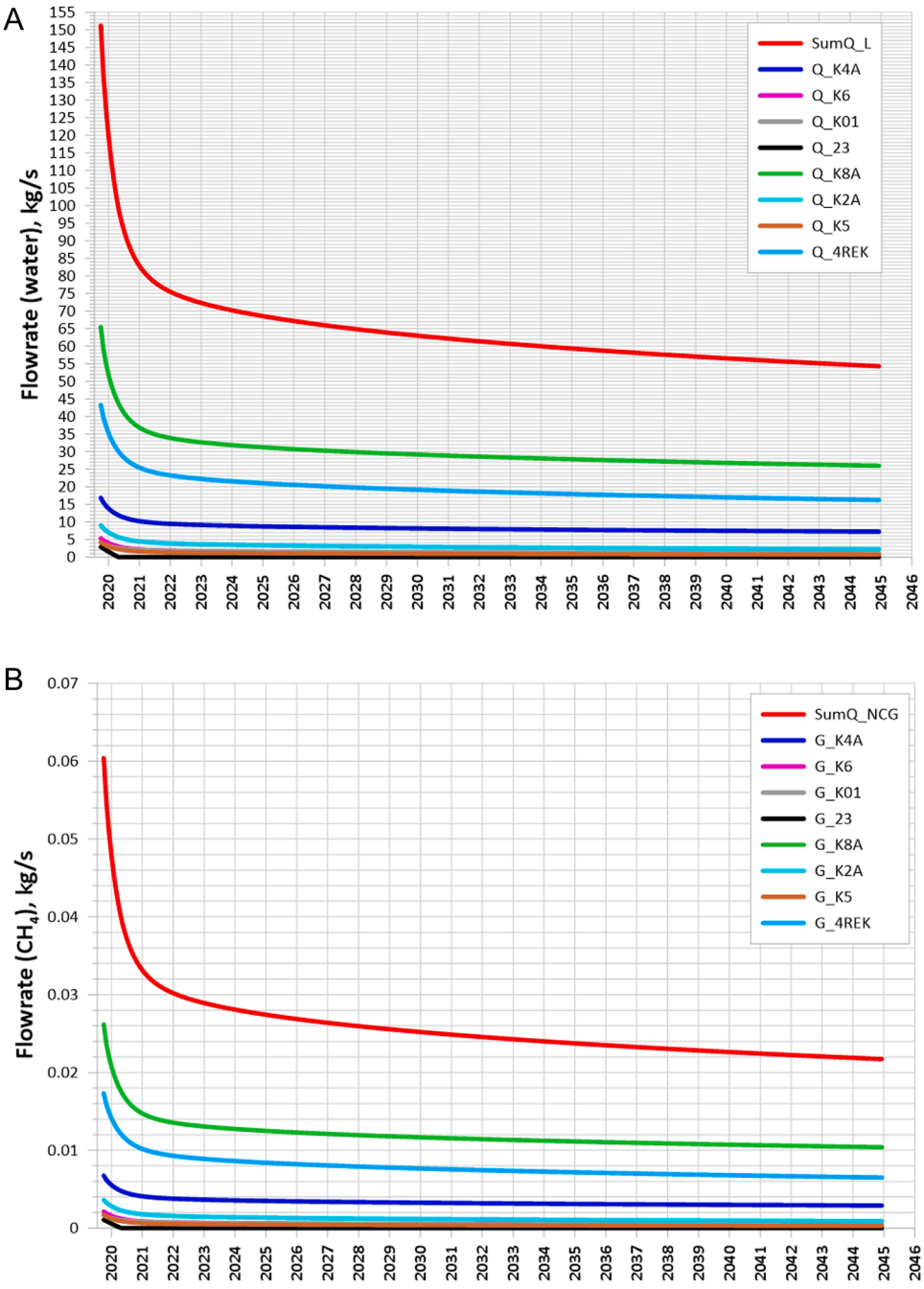

Fig. 16. A Forecast of total and individual thermal water flow rate changes from production wells 23, K6, K01, K5, K4A (2REK), K8A (3REK), K2A, 4REK (Forecast_7 modeling scenario).
B Forecast of total and individual gas component (CH_4) flow rate changes from production wells 23, K6, K01, K5, K4A (2REK), K8A (3REK), K2A, 4REK (Forecast_7 modeling scenario).

6.5. Predictive modeling of operation of existing and additional production wells with re-injection (151.5 kg/s)

The considered scenario differs from the preceding one by addition of three reinjection wells (R1, R2, R3) with injection intervals at −1600 to −1500 m and placed in 5198 (R1), 5337 (R2), 5106 (R3) model elements located on faults continuation 1, 2 and 3 (Fig. 14). Each of the reinjection wells is given a fluid flow rate of 50.5 kg/s and a salinity of 10 g/L with an enthalpy of 126 kJ/kg.

Fig. 17 shows predicted changes in temperature, thermal water flow rate, gas component flow rate (CH_4) and changes in salinity (g/l) from production wells 23, K6, K01, K5, K4A (2REK), K8A (3REK), K2A, 4REK (Forecast_7R modeling scenario).

According to the forecast modeling, during the estimated period of 25-year operation from 2021 to 2045, the temperature in production wells 23, K6, K01, K5, K4A (2REK), K8A (3REK), K2A, 4REK will not change significantly (changes to +−2 °C) (Fig. 17A). Total thermal water flow rate from production wells will be 175.5 kg/s at the beginning of the forecast operational period and will slightly decrease to 164.9 kg/s (−6.0%) (Fig. 17B), total gas component (CH_4) flow rate from production wells will decrease from 70.1 g/s to 59.5 g/s (−15.1%) (Fig. 17C). At the same time the highest individual productivity from 18 to 73 kg/s will have wells K4A (2REK), K8A (3REK), 4REK. Wells K2A, K6, K01, K5, 23 will have low productivity up to 5–10 kg/s each. Changes in M salinity are generally insignificant (−0.2 to 0.6 g/L), with decreasing M predicted for well 23, K01, K4A (2REK), and 4REK, while wells K6, K5, K8A (3REK), and K2A are predicted to slightly increase M (Fig. 17D). As in the previous modeling scenario, wells distant from the discharge area and characterized by high productivity indices will show the highest productivity at the end of the operation period. But, unlike

the previous scenarios, re-injection ensures stable water withdrawal rate for the whole forecast operation period.

7. Conclusions

1 The Ketkinsky geothermal field appears to be the product of magma and water injection from the Koryaksky volcano. Although in the range of drilling by wells to a depth of 2.4 km the axis of thermal anomaly dips in the SSE direction, the gradients of fluid pressure and gas content CH_4 (thermogenic origin) are directed to the ENE. Actual thermal recharge (according to seismic data) may be carried out by magma injections in the form of sills in the depth range from −5 to −2 km from the SW sector of the Koryaksky volcano. The water recharge according to the data of the water isotope composition is mixed: it is carried out through the structure of the Koryaksky volcano from above 2 km and at the expense of buried waters of marine origin, accumulated in the Neogene-Paleogene and Cretaceous basement sediments. The system of the identified productive faults is geometrically conjugated with the proposed above scheme of the thermal and water recharge of the Ketkinsky production reservoir.

2 The hydrogeological model of the Ketkinsky geothermal field was created as a digital model having a volume of 7 km x 5 km x 2.5 km (from the topographic surface), it includes the space drilled by exploration and production wells. The model is based on 3D distributions of temperature, pressure, salinity and CH_4 content, geometry of productive faults and well productivity characteristics. The model space was zoned with separation of deep and shallow productive

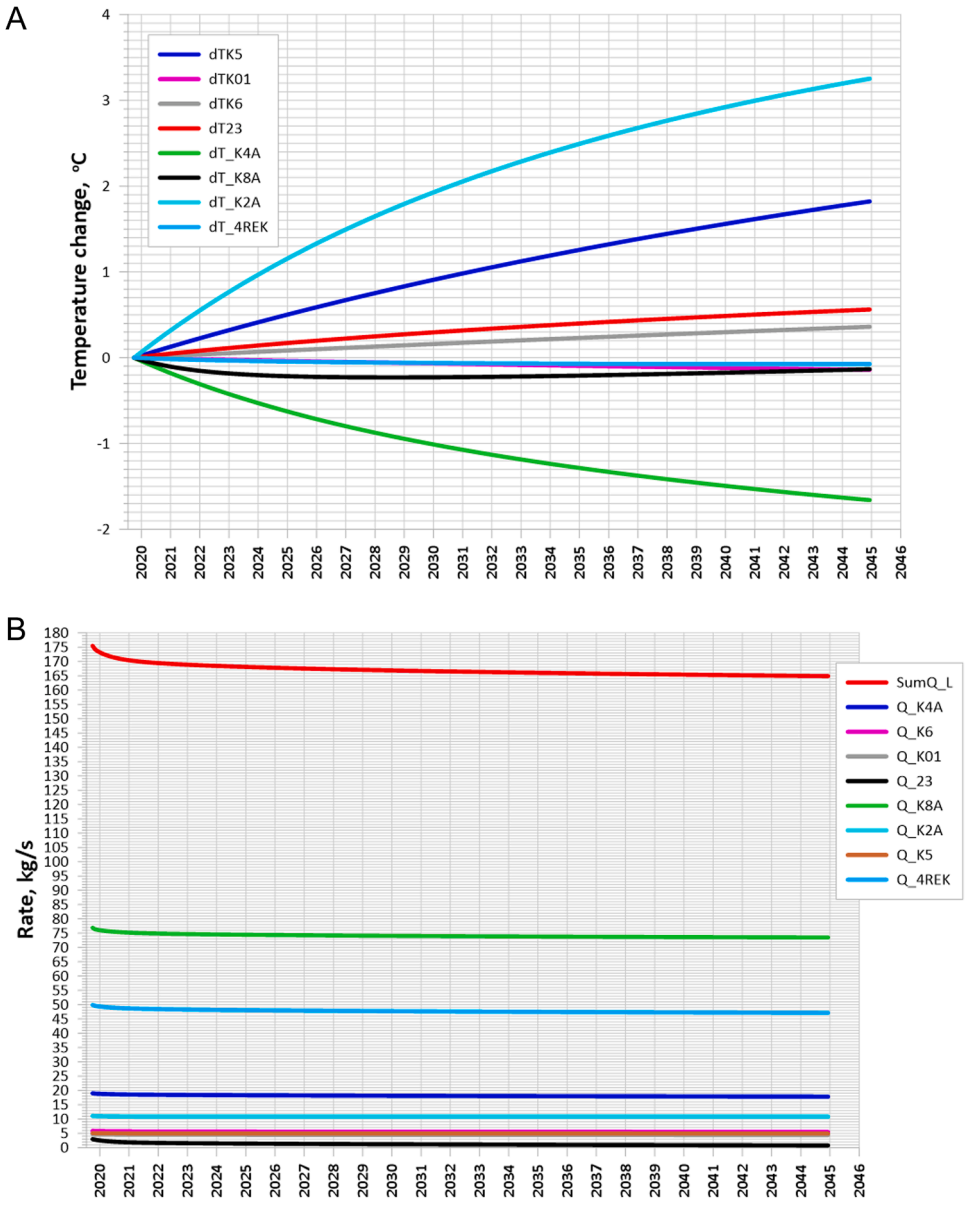

Fig. 17. **A** Prediction of reservoir temperature changes in model elements corresponding to production zones of production wells 23, K6, K01, K5, K4A (2REK), K8A (3REK), K2A, 4REK (Forecast_7R modeling scenario).
B Forecast of total and individual thermal water flowrate changes from production wells 23, K6, K01, K5, K4A (2REK), K8A (3REK), K2A, 4REK (Forecast_7R modeling scenario).
C Forecast of total and individual gas component (CH_4) flow rate changes from production wells 23, K6, K01, K5, K4A (2REK), K8A (3REK), K2A, 4REK (Forecast_7R modeling scenario).
D Forecast of changes in salinity of production wells 23, K6, K01, K5, K4A (2REK), K8A (3REK), K2A, 4REK (Forecast_7R modeling scenario).

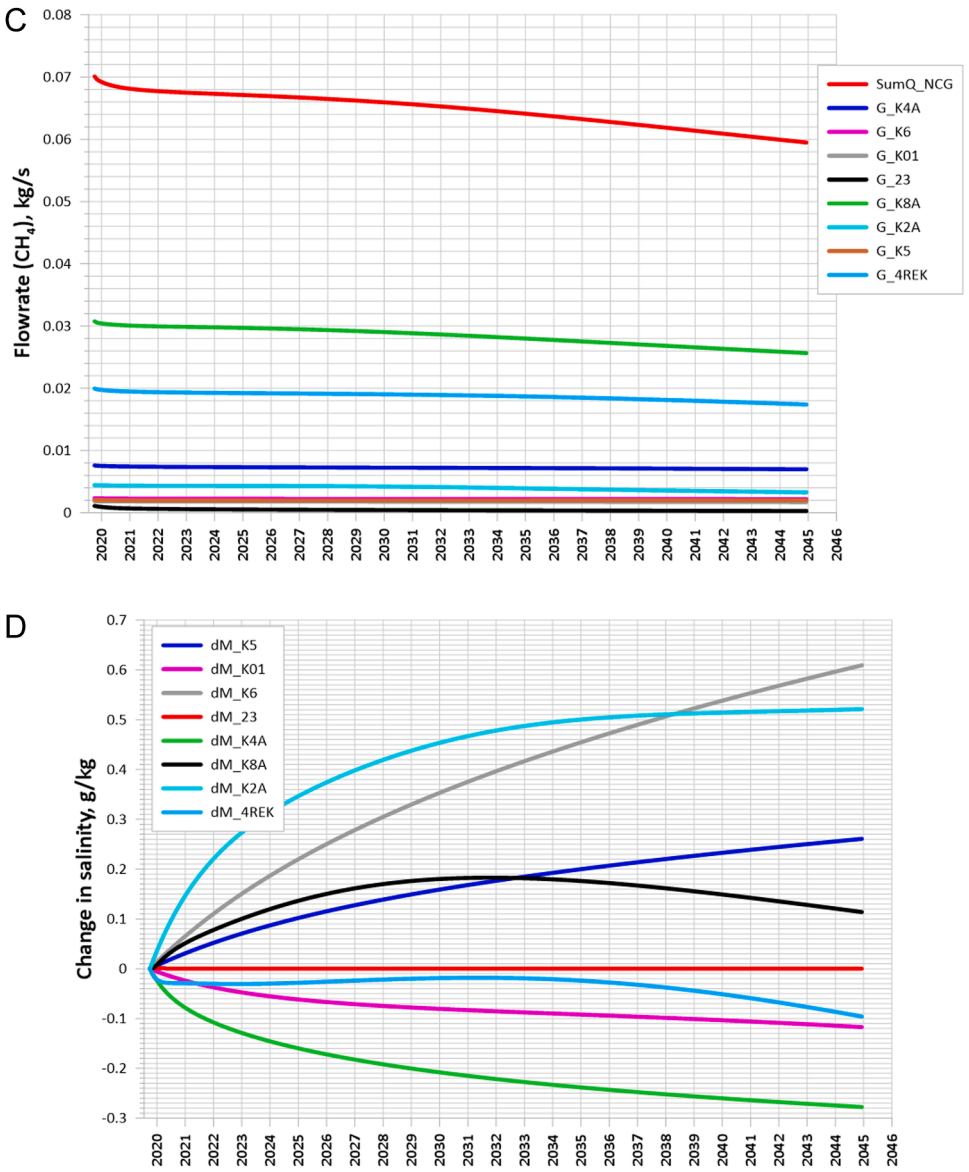

Fig. 17. (*continued*).

geothermal reservoirs, the area of deep upflow in the SSE part of the model base and the shallow area of thermal fluid discharge.

3 Inversion iTOUGH2-EWASG simulation of the natural state (using existing 3D temperature, pressure, CH_4 mass fractions and salinity as initiial conditions data) was used to estimate the thermal fluid upflow and the permeability of productive geothermal reservoirs. Bottomhole temperatures after drilling, pressures in productive well intervals, and thermal fluid salinity of discharging wells were used as calibration data (11 calibration points each). Thermal fluid upflow rate is estimated to be about 10 kg/s, permeability is estimated to be 190 mD (shallow production reservoir) and 35 mD (deep production reservoir).

4 Inversion iTOUGH2-EWASG modeling of the hydrodynamic exploitation history was used to estimate the compressibility of productive geothermal reservoirs. Level change data from observation wells K1, K2, K5, and Z3 from 07.1989 to 10.1993 were used for model calibration. The compressibility of the deep reservoir is estimated at 7.16E-10 Pa^{-1}, the shallow reservoir at 4.14E-07 Pa^{-1}. Direct modeling with the above parameters reproduces the exploitation history of salinity and temperature changes in production wells.

5 Forecast modeling of the operation of existing and additional production wells with assigned constant total flow rate of 53.6 kg/s for the 25-year period shows a pressure reduction in the productive reservoirs at the end of operation from 1.7 bar (shallow reservoir) to 5.6 bar (deep reservoir) (Forecast_1). This will prevent wells from operating in a self-discharge conditions.

6 Forecast modeling of the operation of existing production wells 23, K6, K01, K5 for the 25-year period with submersible pumps at immersion depth of 70 m (current PI were assigned) shows that the total flow rates from these production wells will slowly decrease from 18.9 to 14.2 kg/s (water) and from 7.5 g/s to 5.7 g/s (gas, CH_4), while no significant changes in temperature and salinity are expected (Forecast_6). These flowrates values may correspond to the operational reserves of category B + C1 (Instructions, 1984).

7 Forecast modeling of existing (23, K6, K01, K5) and re-drilled (K4A (2REK), K8A (3REK), K2A, 4REK) production wells for the 25-year period with submersible pumps at immersion depth of 70 m (initial PI for re-drilled wells were assigned) shows that the total flow rates from these production wells will decrease from 151.2 kg/*sec* to 54.3 kg/s (water) and from 60.4 g/s to 21.7 g/s (gas, CH_4), while no significant changes in temperature and salinity are expected for all

wells except for well 23 (Forecast_7). These flowrates values may correspond to the operational reserves of category B + C1+C2 (Instructions, 1984).

8 The use of submersible pumps and re-injection can significantly increase the reserves of Ketkinsky field to 165–175 kg/s with a temperature of 70–80 °C and 60–70 g/s of CH_4 (Forecast_7R). Additional production output may be achieved by directional drilling targeted to: (1) Productive faults (1,2,3)) and known thermal anomaly in the SSE sector of the field; (2) In the area between Ketkinsky geothermal field and Koryaksky volcano.

9 Linear relationship between flowrates and level drawdown in a deep production wells (K8, K6, K01, K4A) suggest two-phase conditions in a deep reservoir, while estimated feed zone pressures in those wells are above bubbling pressure. That's mean possibility of CH_4 content underestimation in a deep production reservoir with a factor range from 3 to 8 and this increase potential CH_4 productivity of Ketkinsky geothermal field as a whole.

Authors contribution

A.V. Kiryukhin: Conceptualization, Methodology, Modeling, Validation, Data curation. **I.N. Nazhalova:** Data curation. **N.B. Zhuravlev:** Data curation.

Declaration of Competing Interest

The authors declare that they have no known competing financial interests or personal relationships that could have appeared to influence the work reported in this paper.

Data Availability

The data that has been used is confidential.

Acknowledgement

The authors are grateful to V.A. Ustimenko, Director of JSC "Zarechnoye", for the support of the work performed, A. Battistelli for consultations on the application of TOUGH2-EWASG. Authors appreciated three unknown reviewer's comments and suggestions, which help a lot to improve manuscript of this paper.

Funding

This study was funded by RFBR and JSPS according to research project # 21–55–50003.

References

Battistelli, A., Calore, C., Pruess, K., 1997. The simulator TOUGH2/EWASG for modeling geothermal reservoirs with brines and non-condensible gas. Geothermics Vol. 26 (No. 4), 437–464.

Etiope, G., Lollar, B.S, 2013. Abiotic methane on earth. Rev. Geophys. 51, 276–299. https://doi.org/10.1002/rog.20011.

Finsterle, S, 1999. iTOUGH2 User's Guide //Report LBNL–40040. Berkeley, CA, USA, p. 130.

Finsterle, S, 2014. iTOUGH2 V7.0 Command Reference. Rep. LBNL–40041 Rev. Lawrence Berkeley Natl. Lab., Berkeley, California.

Instructions for the Application of the Classification of Operational Groundwater Reserves for Thermal Power Water Deposits State reserves commitee 1984, 15 p. (in Russian).

Kiryukhin, P.A., Kiryukhin, A.V., 2016. Frac-Digger. Certificate of state registration of computer programs # 2016612168 of 21.06. 2016.

Kiryukhin, P.A., Kiryukhin, A.V., 2017. Frac-Digger2. Certificate of state registration of computer programs # 2017618050 of 21.09.2017.

Kiryukhin, A.V., Asaulova, N.P., Finsterle, S., 2008. Inverse Modeling and Forecasting For the Exploitation of the Pauzhetsky geothermal Field. Geothermics, Kamchatka, Russia, pp. 540–562. V. 37.

Kiryukhin A. V., Kiryukhin V. A., Manukhin Yu. F. Hydrogeology of volcanogenes. - SPb.: Nauka, 2010. 395 p. (in Russian).

Kiryukhin, A.V., Vorozheikina, L.A., Voronin, P.O., Kiryukhin, P.A., 2017a. Thermal-Permeability Structure and Recharge Conditions of the Low Temperature Paratunsky geothermal Reservoirs, 70. //Geothermics, Kamchatka, Russia, pp. 47–61.

Kiryukhin, A., Lavrushin, V., Kiryukhin, P., Voronin, P., 2017b. Geofluid Systems of Koryaksky–Avachinsky Volcanoes (Kamchatka, Russia). //Geofluids, p. 21. https://doi.org/10.1155/2017/4279652. Vol. 2017, Article ID 4279652.

Kiryukhin, A.V., Polyakov, A.Y, Usacheva, O.O, Kiryukhin, P.A., 2018. Thermal-permeability structure and recharge conditions of the Mutnovsky high temperature geothermal field (Kamchatka, Russia). Journal of Volcanology and Geothermal Research 365, 36–55. https://doi.org/10.1016/j.jvolgeores.2018.02.010.

Kiryukhin, A., Voronin, P., Zhuravlev, N., Kopylova, G., 2021. Water-methane geothermal reservoirs in a south-west foothills of Koryaksky volcano. In: Kamchatka PROCEEDINGS. 46th Workshop on Geothermal Reservoir Engineering Stanford University, Stanford, California, pp. 320–325. February 15-17.

Kiryukhin, A.V., 2020. Geothermofluidomechanics of Hydrothermal, Volcanic and Hydrocarbon Systems. Eko-Vector I-P (in Russian). Ed: St. Petersburg. https://www.elibrary.ru/item.asp?id=45739830.

Maltseva, K.I., Kotelnikova, T.K., Nazhalova, I.N., 2011. Report On "Calculation of Reserves of Thermal Waters of Ketkinsky deposit (as of December 31, 2010)" Under the Contract Number 29/10 of 20.09.2010. (in 2 books). Yelizovo, p. 262 (in Russian).

Netesov Yu. A., 1989. Report on detailed searches for thermal waters in the Ketkinsky section of the Pinachevskaya geothermal area in 1986-1988. (geophysical works). (in Russian).

Nurmukhamedov, A.G., Netesov, Y.A., 1984. Report on geophysical works conducted by the 2nd Ketkinsky party in 1982-1984. Pinachevskaya Square (in Russian).

Nurmukhamedov, A.G., Popruzhenko, S.V., 1989. Report on general searches for thermal waters in the northwestern part of the Petropavlovsk geothermal area, Stage I - geophysical works 1987-1989. (№-57-89-A, B, C, D; "-57-101-A, B; №-57-102-A). Yelizovskaya Party. r. (in Russian).

Pozdeev, A.I., 2003. Hydrocarbon gas generation of the Avacha Depression, its prospects and relationship with seismicity. //Volcanology and Seismology. № 6. - C. 44-54 (in Russian).

Pruess, K., Oldenburg, C., Moridis, G., 1999. TOUGH2 User's guide, Version 2.0. Rep. LBNL–43134. Lawrence Berkeley Natl. Lab., Berkeley, California.

Shymanovich, V.M., Yasoveyev, M.G., 1989. Density and Viscosity Characteristics of Hydrogeological Section of Pripyat Trough. //Oil and Gas Geology, pp. 41–45. http://geolib.ru/OilGasGeo/1989/02/Stat/stat12.html (in Russian).

Taran, Yu.A., Ryabinin, G.V., Pokrovskii, B.G., Nazhalova, I.N., Malik, N.A, 2021. Mineral Waters of the Avachinskaya Depression, Kamchatka, 2021 Vestnik KRAUNTS. SCIENCE OF EARTH. № 2. V. 50 (in Russian).

Zadirey, A.V., 1984. Report on geophysical works conducted by the 1st Ketka party in 1980-1982. Pinachevskaya Area. r. (in Russian).

Zippa E.V. Geochemistry of Thermal Waters in Jiangxi Province (China). Author's abstract of the thesis for the degree of Candidate of Geological and Mineralogical Sciences in the specialty 25.00.07 - hydrogeology, Tomsk, 2020 (in Russian).